Seminar Work Report

Magnetocaloric effect of $Ni_2Mn(Ga,Bi)$ shape memory alloys

José Carlos Vieira Leitão

Universidade de Aveiro

Aveiro, July 2007

Acknowledgments

The author of the current report would like to acknowledge the collaboration and precious support of the Magnetocaloric Effect group of the University of Aveiro, Dr. Vitor Brás de Sequeira Amaral (seminar coordinator), Dr. Mario de Souza Reis (seminar co-coordinator), Prof. Joaquim Vieira, Dr. Daniel Rocco, M.Sc João Amaral, M.Sc. Rodrigo Pacher Fernandes and Lic. Nuno Fernandes from the University of Aveiro.

Abstract

The magnetocaloric effect (MCE) is the best chance at creating a more efficient refrigeration technique, both in energy and environmental friendliness.

The MCE is characterized as a change of either temperature or entropy in a magnetic material due to a change of magnetic field. This change is maximum around the material's T_c (Curie Temperature) in ferromagnets. As such the main concern in the study of the MCE is the search for materials with large MCE (mainly characterized by a great magnetic entropy variation) in a wide temperature range around room temperature (RT). The wideness is characterized by the relative cooling power (RCP).

Thus, this work focuses on the widely studied Heusler alloy and the influence of bismuth alloying in the stoichiometry $Ni_2Mn(Ga_{1-x}Bi_x)$ in an attempt to merge the magnetic and structural transitions, T_c and T_M respectively, in order to create a giant magnetocaloric effect (GMCE).

Following this, we produced six samples (x=0;0,1;0,2;0,3;0,4;0,5) and studied their magnetic properties. After preparation, however, it was found that only one pure phase sample was produced and suitable for study (x=0), having revealed an average magnetic entropy change of ΔS=-1.29 $Jkg^{-1}K^{-1}$ for the magnetic transition with RCP_m=36.2 J/kg

at T_c=385 K J/kg and ΔS=4.7 $Jkg^{-1}K^{-1}$ for the structural transition at T_M=193.3 K with RCP_s=18.08 J/kg.

This result showed agreement with previous literature data and future work can then proceed with the study of bismuth's solubility limit and a new set of $Ni_2Mn(Ga_{1-x},Bi_x)$ alloys, with a much lower concentration of bismuth. As such, with good samples with Bi we can proceed with the magnetocaloric studies for this series.

Contents

List of Figures

List of Tables

Chapter 1

Introduction

In all of history there has been a desire to control environmental temperature, whether be it for food conservation or simple comfort. Food conservation is without a doubt the most important aspect and in simple terms, it is impossible to conceive modern society without refrigerators and food preservation.

Refrigerators first came about in the early 20^{th} century. Mainly those operated with the vapor-compression method, using steam engines with open drive compressors, subjected to leaking noxious or dangerous refrigerants. Those where too big, dangerous and expensive for a wide range distribution. [1]

Later, in 1930, this system evolved and the use of CFCs (Chlorofluorocarbons) in refrigeration appeared, rapidly dominating the market. Latter research revealed that the use of uncontrolled CFCs damaged the stratospheric ozone layer. As such, and due to the Montreal protocol, the use of CFCs was substituted by HFCs, that, although, do not damage the ozone layer but contribute to the rise of the earth's average temperature and the greenhouse effect phenomenon, reveling the HFCs as environmentally harmful. Both

CFCs and HFCs were targeted by the Kyoto protocol and governments around the world committed to reduce the use of these gases [2].

One other important point of the Kyoto Protocol is energy efficiency. Electric consumption represents one fifth of the total energy used in Europe [3]. Thus, knowing that modern day refrigerators work well below the optimal Carnot cycle [4], the improvement of this technology has to reflect both efficiency and environmental friendliness.Thus magnetic refrigeration, based on the magnetocaloric effect, comes into play. This technology uses materials in solid form, without the use of hazardous gases, and can reach a maximum efficiency of about 60% [3], being a bright promise for the future.

The Magnetocaloric Effect (MCE), discovered in 1881 by E. Warburg [5], has revealed an exciting and promising propriety of magnetic materials. This effect can be seen from either an adiabatic or an isothermal process; both due to a change of the applied magnetic field. In the adiabatic process, the magnetic material changes its temperature, whereas in the isothermal process, the magnetic material exchanges heat with a thermal reservoir. From the quantitative point of view, the MCE is measured trough the isothermal magnetic entropy change (ΔS) or adiabatic temperature change (ΔT_{ad}); both quantities derived from thermodynamic relationships and, to obtain those, the measurement of magnetization and specific heat as a function of temperature and magnetic field are needed.

It is straightforward the idea to produce a thermo-magnetic cycle based on the isothermal and/or adiabatic processes, using therefore the Brayton and Ericsson cycles, respectively; and indeed this idea begun in the late 1920s, when cooling via adiabatic demagne-

tization was proposed by Debye [6] and Giauque [7]. The process was after demonstrated by Giauque and MacDougall, in 1933; where they reached 250 mK [8]. Since then, the adiabatic demagnetization was used within some specific contexts; namely, to cool NASA-XRS detectors (1.5 K).

On the other hand, room temperature magnetic cooling device technology is still in an early phase of development, with no commercially available products and only few prototypes. In August 2001, Astronautics Corporation of America, USA, announced a prototype of room temperature magnetic cooler. This prototype has a cooling power of 95W, and uses as the active magnetic material Gd spheres [9]. Later, in March 2003, Chubu Electric and Toshiba, Japan, also announced the creation of a room temperature magnetic cooler prototype. This machine has a cooling power of 60W, and uses a layered bed of a Gd-Dy alloy as the active magnetic material [9]. Both of them used permanent magnets of Nd-Fe-B to produce the magnetic field.

However, nowadays, the magnetic materials available and studied by the scientific community do not have the needed characteristics to be used in large scale commercial use, due to technological and/or economic restrictions. For a successful application, we need a material of low cost, non-toxic with good thermal conductivity and with a huge and broad ΔS variation vs. temperature (maximum around the magnetic phase transition). In this sense, most of the research developed world wide is devoted to explore and optimize the magnetocaloric properties of known materials, as well to seek for new magnetocaloric characteristics in new materials.

Chapter 2

Magnetic Basis Behind the Magnetocaloric Effect

2.1 Classes of Magnetic Materials

Magnetic properties in matter usually originate from the interaction between the spins in the incomplete shells of atoms. The nature of the several known classes of magnetic materials is defined by this interaction.

For the current report we will describe two classes of magnetic materials: paramagnetism and ferromagnetism; both of them important to the magnetocaloric effect. The most prominent characteristics of the ferromagnetism is the fact that there is a natural alignment in spins, due to a positive exchange interaction between spins. This natural alignment occurs only below the Curie temperature T_c of the system, above which the ferromagnetic material behaves like a paramagnetic one [10]. The paramagnetism is essentially characterized by the fact that, although the spin interaction is still present, the

competition of this factor with the thermic fluctuations will result in a null average for T>T_c in a magnetic field of 0T, presenting themselves naturally unaligned. It implicates that these materials have zero total magnetization, unless when in the presence of an applied magnetic field that forces the alignment of the spins [10].

2.2 Magnetization

Lets consider a system of non-interactive magnetic ions (or atoms) subjected to a magnetic field H, the magnetization of a given material is the sum of all individual magnetic moment divided by its volume or mass.

The thermal average of the magnetization is given by a weighted average over all possible projections μ_z of the individual magnetic moment μ. This projection μ_z is related to the eigenvalue of the spin operator J through:

$$\mu_z = g\mu_B m_J \tag{2.1}$$

Where $m_J = -J, -J+1, ..., +J-1, +J$, g is the Landé g-factor and μ_B the Bohr magneton (9.27×10^{-24} JT^{-1}).

The mentioned weight is given by the Boltzmann factor:

$$P(m_J) = \frac{\exp(-\mathcal{H}/k_B T)}{Z} \tag{2.2}$$

Where k_B is the Boltzmann constant (1.38×10^{-23} JK^{-1}), Z ($= \sum_{m_J} \exp(-\mathcal{H}/k_B T)$) is the partition function of the system and $\mathcal{H}$ stands for the Hamiltonian that in the present

case is given by only the Zeeman energy:

$$\mathcal{H} = -\mu B = -g\mu_B B m_J \tag{2.3}$$

Thus,

$$< \mu_z >= M = \sum_{m_J} \mu_z P_{m_J} = g\mu_B \frac{\sum_{m_J} m_J \exp(g\mu_B B m_J / k_B T)}{\sum_{m_J} \exp(g\mu_B B m_J / k_B T)} \tag{2.4}$$

Development of the above equation, in Appendix A, considering multiple ions and putting the Magnetization in units of μ_B, leads to:

$$M = ngJB_J(x) \tag{2.5}$$

Being n the number of ions per volume and B_J the Brillouin function, given by:

$$B_J(x) = \left(1 + \frac{1}{2J}\right)\left[\coth\left(1 + \frac{1}{2J}\right)x\right] - \frac{1}{2J}\coth\left(\frac{x}{2J}\right) \tag{2.6}$$

Where x is:

$$x = \frac{g\mu_B JB}{k_B T} \tag{2.7}$$

2.2.1 Paramagnetism

In the Paramagnetic case we have that the magnetic field H is the same as the external field. It is important to emphasize that there are no exchange interaction between spins and this fact characterizes the paramagnetic material.

Thus in a paramagnetic material the magnetization increases with the application of an external magnetic field, as observed in Figure (2.1). For calculation purposes, either for Figure (2.1) or any other that involves these values in the calculations, the total spin J has been considered $\frac{3}{2}$ and g=2.

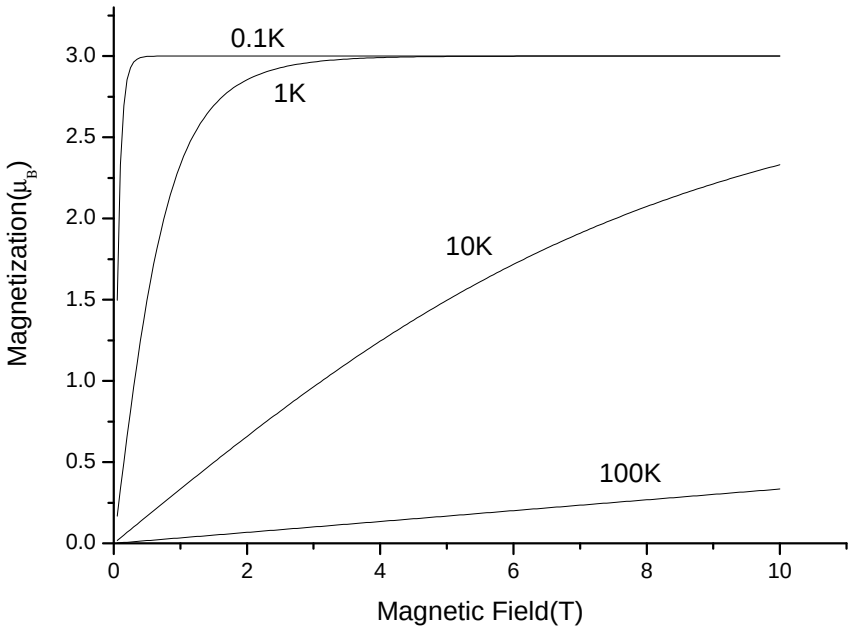

Figure 2.1: Magnetization as a function of magnetic field for several temperatures in a paramagnetic material, with $J = \frac{3}{2}$ and $g = 2$

The above graph, has been numerically calculated using a routine created by the author in the program MatLab, using the Brillouin function Eq.(2.6) and Eq.(2.5), and plotted using the program Origin.

2.2.2 Ferromagnetism

Now we consider the case where there are (positive) exchange interaction leading to ferromagnetism at low enough temperatures.

Besides the Zeeman term one considers the exchange between two negative moments summed over the whole sample.

$$\mathcal{H}_{int} = -J \sum \overrightarrow{\mu_i} \cdot \overrightarrow{\mu_j} \tag{2.8}$$

Considering the mean field approximation, the magnetic field of Eq.(2.7) can be substituted by an effective field, that is a simple sum of the external field H_{ext} and the "magnetic field" created by the magnetization of the ferromagnetic material. Thus:

$$H \rightarrow H_{ef} = H_{ext} + \lambda M \tag{2.9}$$

Where λ is the mean field parameter.

Expanding the $\coth(x)$ for small x, and then replacing the result in the Brillouin function, equation (2.6), we obtain:

$$B_J \approx \frac{J+1}{3J} x \tag{2.10}$$

Thus,using Eqs.(2.5)(2.7)(2.9) and considering a zero external magnetic field we have:

$$M = g^2 \mu_B^2 J \frac{(J+1)}{3kTc} \lambda M \tag{2.11}$$

and, consequently:

$$Tc = \frac{g^2 \mu_B^2 n \lambda J(J+1)}{3k} \tag{2.12}$$

This is the analogue expression for the Curie temperature of a ferromagnetic material, above which there is no spontaneous magnetization.

The natural spin alignment of ferromagnetic materials, as stated above, can be destabilized by increasing the temperature, decreasing the magnetization of the ferromagnetic material. This decrease reaches a critic state when temperature reaches the Curie temperature, where magnetization (spin alignment) finally drops to zero and the material then behaves like a Paramagnetic one.

Figure (2.2) summarizes all of the mathematical descriptions above mentioned, where we present magnetization in the mean-field approximation as a function of temperature for the ferromagnetic materials at H=0, solving the equation

$$M = ngJB_J\left(\frac{g\mu_B J}{kT}(\lambda M)\right) \tag{2.13}$$

Note the Curie temperature, below which there is spontaneous spin order and consequent magnetization and zero magnetization above. The calculations for Figure (2.2), were forcefully made numerically, this is due to the magnetization equation in ferromagnetic materials being autodependent in this approximation.

Of particular interest in the ferromagnetic case is the observation of behavior similar to a paramagnetic material above the already referred Curie temperature, as shown in Figure (2.3).

In the presence of an external magnetic field, one has to solve Equation (2.13).

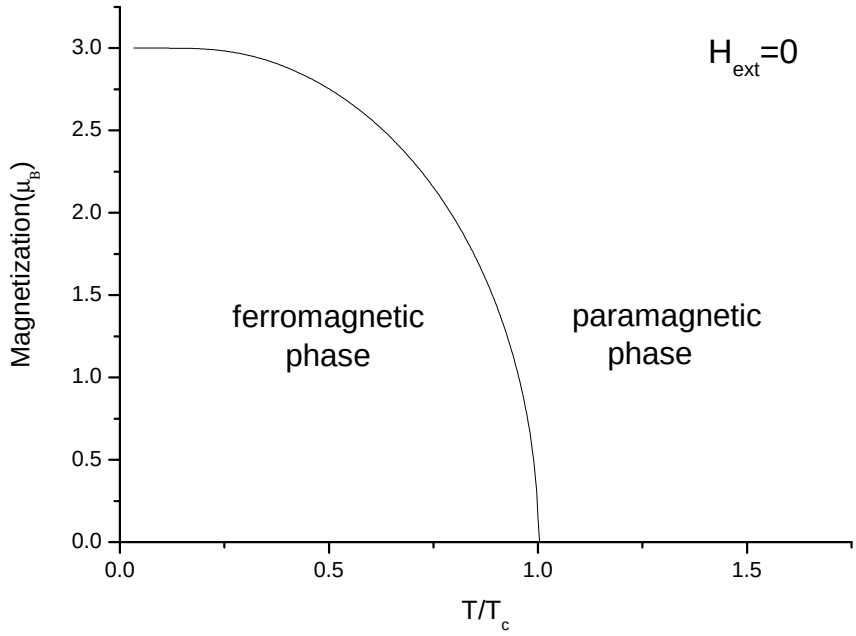

Figure 2.2: Magnetization in order of Temperature showing the magnetization drop in T_c, where the ferromagnetic phase turns paramagnetic

2.3 Magnetic Susceptibility

The Magnetic susceptibility, χ, represents the initial magnetic response of a material to the action of a magnetic field and is another important quantity in magnetism. It is defined by:

$$\chi = \lim_{H \to 0} \frac{\partial M}{\partial H} \tag{2.14}$$

2.3.1 Paramagnetism

Using equation (2.10) we find that the magnetization in the paramagnetic case is equal to:

$$M = \frac{C}{T} H \tag{2.15}$$

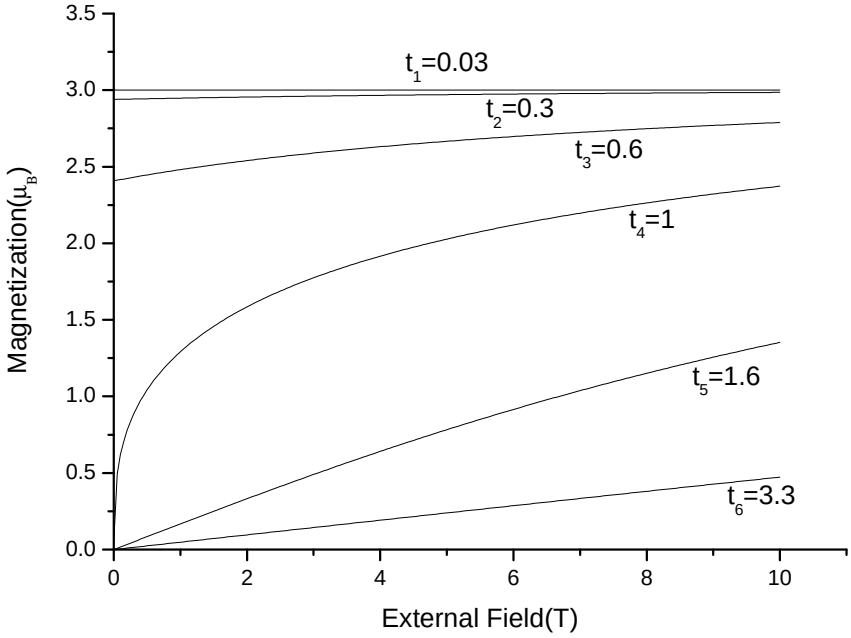

Figure 2.3: Magnetization in order of Magnetic field for several temperatures in a Ferromagnetic material, being $t = T/T_c$

From the development of equations (2.5)(2.6)(2.7) and (2.14), we obtain the following expression for magnetic susceptibility:

$$\chi = \frac{C}{T} \tag{2.16}$$

Where the Curie constant is

$$C = \frac{\mu_0 n g^2 \mu_B^2 J(J+1)}{3k_B} \tag{2.17}$$

For the paramagnetic case, as stated before, the magnetic susceptibility in inversely proportional to the temperature. Figure (2.4) clarifies this idea.

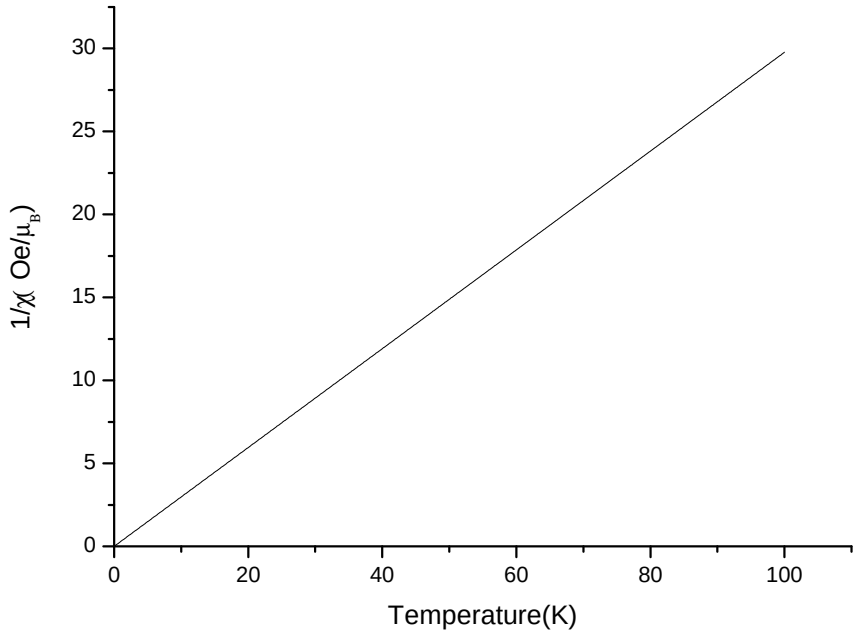

Figure 2.4: The Curie Law for low magnetic field

2.3.2 Ferromagnetism

Similar behavior to the above is displayed by a ferromagnetic material above the Curie temperature, where, reminding again, these materials behave like paramagnetic ones, which means that that for a zero applied magnetic field, their magnetization is zero.

Following a parallel path to the previous, but remembering that the magnetic field is an effective field in the ferromagnetic case ($H_{ef} = H_{ext} + \lambda M$), we obtain the following (using the expression (2.10) of the Brillouin function):

$$M = \frac{C}{T}(H_{ext} + \lambda M) \tag{2.18}$$

and

$$M = \frac{CH_{ext}}{T - C\lambda} \tag{2.19}$$

resulting therefore in the following expression for magnetic susceptibility:

$$\chi = \frac{C}{T - C\lambda} = \frac{C}{T - \theta_P} \tag{2.20}$$

Where θ_P is the paramagnetic Curie temperature, given by:

$$\theta_P = C\lambda \tag{2.21}$$

This behavior is known as the Curie-Wiess law, described by Figure (2.5).

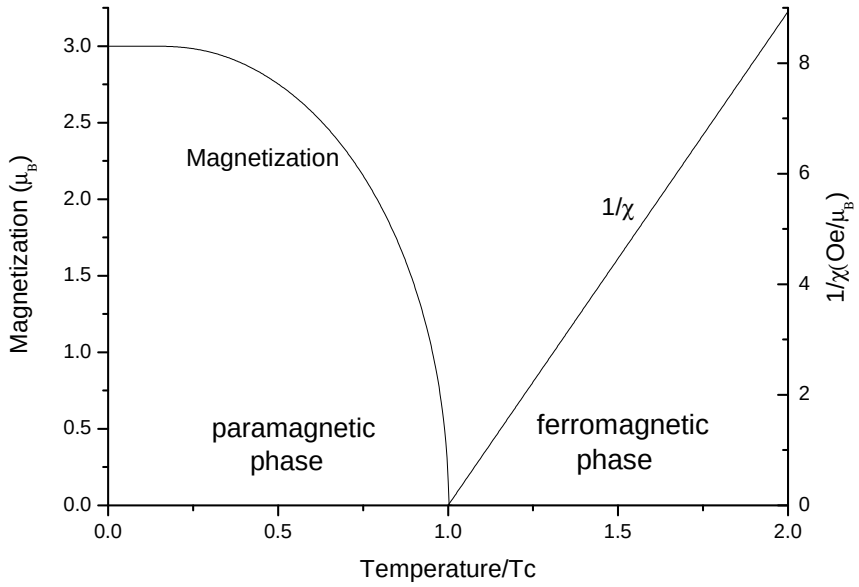

Figure 2.5: The Curie-Wiess Law compared with the fall of Magnetization on a Ferromagnetic material

2.4 Demagnetization Field

A magnetized material, as seen above has aligned spins and, consequently free magnetic poles on its surface. These poles also generate an additional field $\vec{H}_d$ opposite to the

magnetization in the interior of the material, as shown by Figure (2.6):

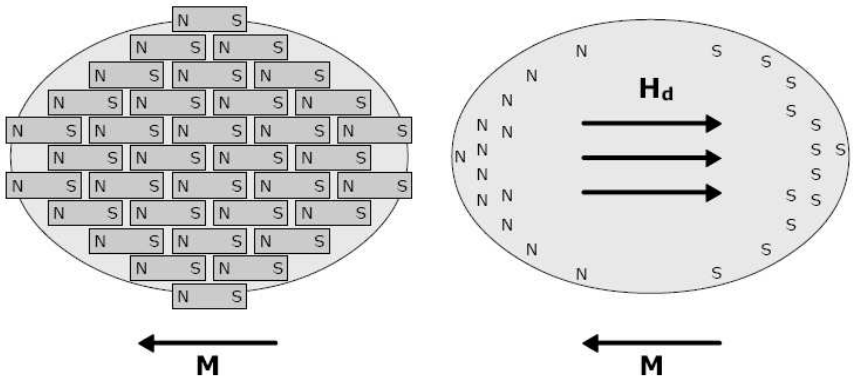

Figure 2.6: Illustration of the magnetization in opposition to the demagnetization field in a magnetic material

Thus, in this light, we should write the total field of a magnetized material as such:

$$\vec{H} = \vec{H_0} - \vec{H_d} \tag{2.22}$$

where $\vec{H_0}$ represents the external applied field and $\vec{H_d}$ is the demagnetization field and can be written as:

$$\vec{H_d} = D\bar{M} \tag{2.23}$$

D is called the demagnetization factor and is related to the geometry of the magnetic material. Considering an uniform magnetization and no external currents in the magnetic material $\vec{H_d}$ may be calculated as such:

$$\vec{H_d} = \frac{1}{4\pi} \oint_S (\vec{M}.\hat{n}) \frac{\vec{r}}{r^3} dS \tag{2.24}$$

where dS represents an element of the integrated surface, $\vec{r}$ its position vector relative to the origin of the system of coordinates, and $\hat{n}$ a unitary vector perpendicular to the surface element of the magnetic material.

Chapter 3

Thermodynamic Basis Behind the Magnetocaloric Effect

3.1 Ideal Thermodynamic Processes

In this section we will cover the thermodynamic processes behind the magnetocaloric effect, being this the change of entropy and temperature with magnetic field, in an isothermal and adiabatic process respectively.

Taking into account the physical meaning of thee magnetism already covered in the previous chapter one understands that when we proceed by applying a field to a magnetic material anchored to a thermal reservoir, this will cause spin alignment, reducing the magnetic entropy. Seeing as temperature remains constant, this will be traduced by a heat transference to the exterior.

Then, by removing the field this process is reversed. This process is illustrated by Figure (3.1).

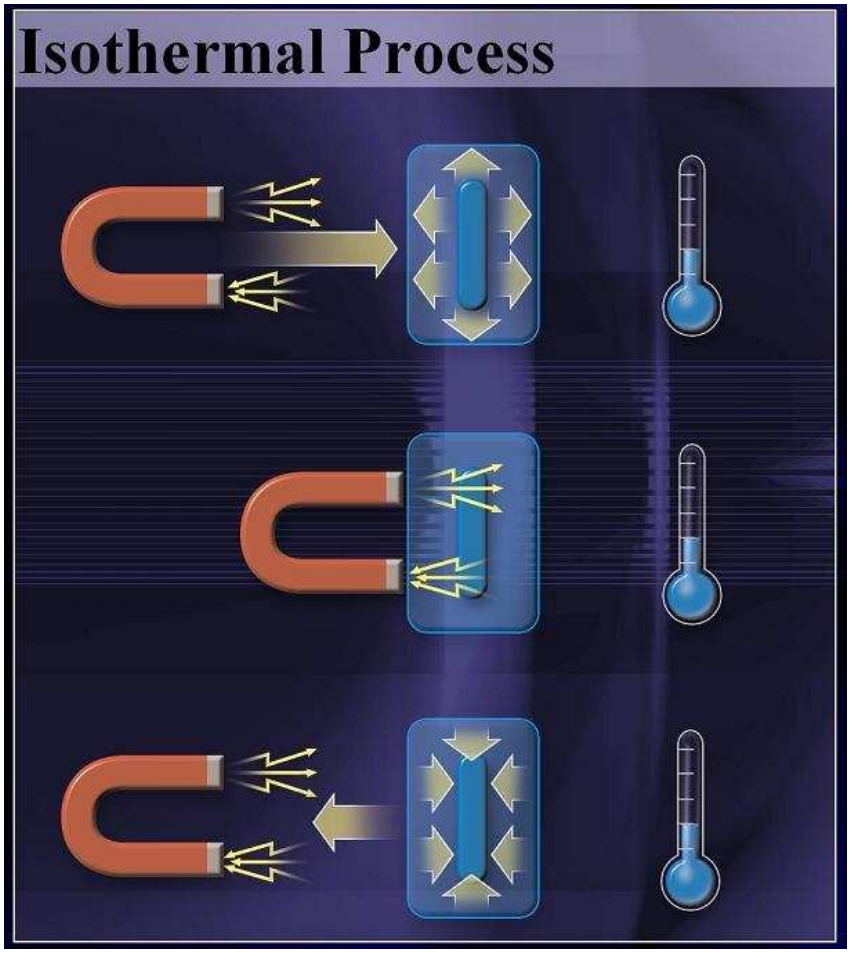

Figure 3.1: Isothermal Process Scheme

To create the temperature variation ΔT of an adiabatic process, again taking into account the magnetism already covered, we proceed by applying a magnetic field to a magnetic material thermally isolated from the exterior. This will again cause a spin alignment and heat is exchanged within the material with the lattice, since the total entropy is constant, resulting in a rise in the temperature of the material. Then, by removing the field the process is reversed.

This process is illustrated by Figure (3.2).

In Figure (3.3) we have a summarization of the above processes

Being the above the bases of the magnetocaloric effect we now have to focus on the

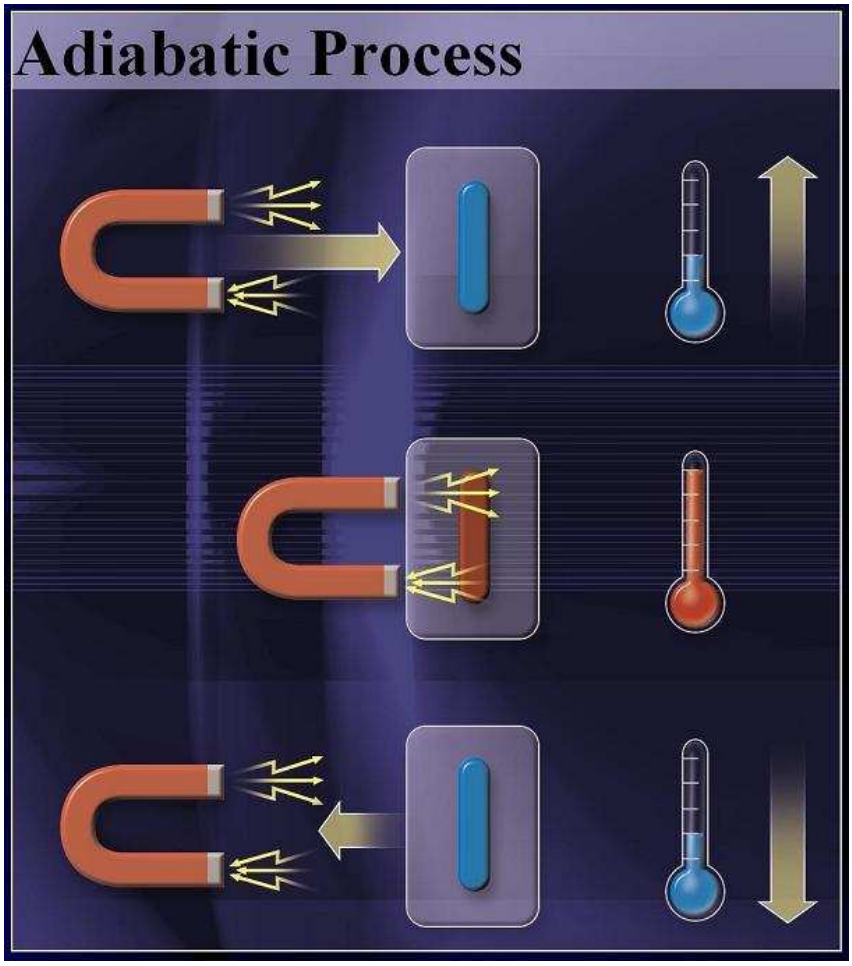

Figure 3.2: Adiabatic Process Scheme

calculation of the ΔS and ΔT, as follows in the next sections.

3.2 Magnetic Entropy Change

Seeing as one of the most important parameters of the magnetocaloric effect is the variation of the magnetic entropy, we will first approach it from a mathematical view, following the same steps as displayed in the book "The Magnetocaloric Effect and its Applications" [11].

Considering the Helmholtz free energy F as a function of magnetic field and temper-

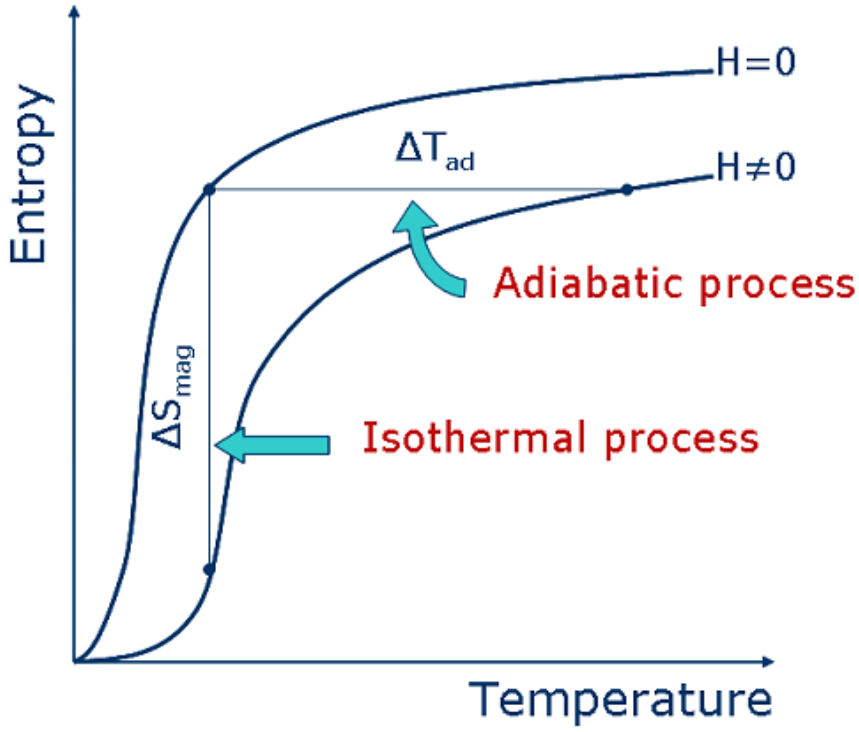

Figure 3.3: Isothermal and Adiabatic Processes

ature, i.e., $F = F(T, H)$, we can write:

$$dF = \left(\frac{\partial F}{\partial T}\right)_H dT + \left(\frac{\partial F}{\partial H}\right)_T dH \tag{3.1}$$

Being

$$F = U - TS \tag{3.2}$$

Where S is the entropy and $U = -MH$ the total energy, we therefore obtain:

$$F = -MH - TS \tag{3.3}$$

However, we defined previously $F = F(T, H)$, thus following from the first law of ther-

modynamics:

$$dF = -SdT - MdH \tag{3.4}$$

Comparing (3.1) and (3.4) we find an expression for the entropy and one other for magnetization:

$$S(T,H) = -\left(\frac{\partial F}{\partial T}\right)_H \tag{3.5}$$

and

$$M(T,H) = -\left(\frac{\partial F}{\partial H}\right)_T \tag{3.6}$$

Thought mathematical development we arrive to:

$$\frac{\partial M}{\partial T} = -\frac{\partial}{\partial H}\left(\frac{\partial F}{\partial T}\right)_H \tag{3.7}$$

and finally to:

$$\left(\frac{\partial S}{\partial H}\right)_T = \left(\frac{\partial M}{\partial T}\right)_H \tag{3.8}$$

that, in order of the entropy change from a field H_i to H_f, is displayed as such:

$$\Delta S(T)_{\Delta H} = \int_{H_i}^{H_f} \left(\frac{\partial M(T,H)}{\partial T}\right)_H dH \tag{3.9}$$

Thus, from the study of the magnetization $M(T,H)$ one can determine ΔS.

One other way of reaching a useful expression for the calculation of the magnetic entropy change is through the specific-heat expression, as follows:

$$C = T\left(\frac{\partial S}{\partial T}\right) \tag{3.10}$$

where, when in order of the entropy we have:

$$\int_0^T \frac{C}{T} dT = S \tag{3.11}$$

as

$$\Delta S = S(H \neq 0) - S(H = 0) \tag{3.12}$$

we finally have:

$$\Delta S = \int_0^T \frac{C(H \neq 0) - C(H = 0)}{T} dT \tag{3.13}$$

As we can see observe, the magnetic entropy variation depends directly on the magnetization $M(H, T)$, that, in it self, depends microscopically on various parameters, such as crystalline structure, spin alignment, charge orbital and many others. Next we will describe, as an example, the simple dependence of the magnetic entropy variation with the spin alignment, using the Brillouin function.

3.2.1 Spin contribution of the magnetic entropy change

In order to calculate the spin influence to the already referred magnetic entropy, we start from the expression for the generalized in a phase space [12]:

$$S = -k_B \sum_i P_{m_J} \ln P_{m_J} \tag{3.14}$$

Where P_{m_J} represents the probability of the system to be in the state m_J.

Development of the above equation to express the spin influence in the entropy, in Appendix B, results in the expression of entropy per spin:

$$S_{spin} = \ln \left(\frac{\sinh \left[x \left(1 + \frac{1}{2J} \right) \right]}{\sinh \left[\frac{x}{2J} \right]} \right) - x B_J(x) \tag{3.15}$$

Being B_J the referred Brillouin function, equation (2.6) and x is equation (2.7).

Following equation (3.15), as we apply a field to a magnetic material its electron spins will align, reducing the entropy, as shown in Figure (3.4).

The entropy variation in the context will then be according to the following:

$$\Delta S_{spin} = S_{spin}(H \neq 0) - S_{spin}(H = 0) \tag{3.16}$$

that is traduced by Figure (3.5)

According to this, considering a Ferromagnetic material, the entropy variation decreases steadily with temperature, until the Curie temperature is reached, from here on

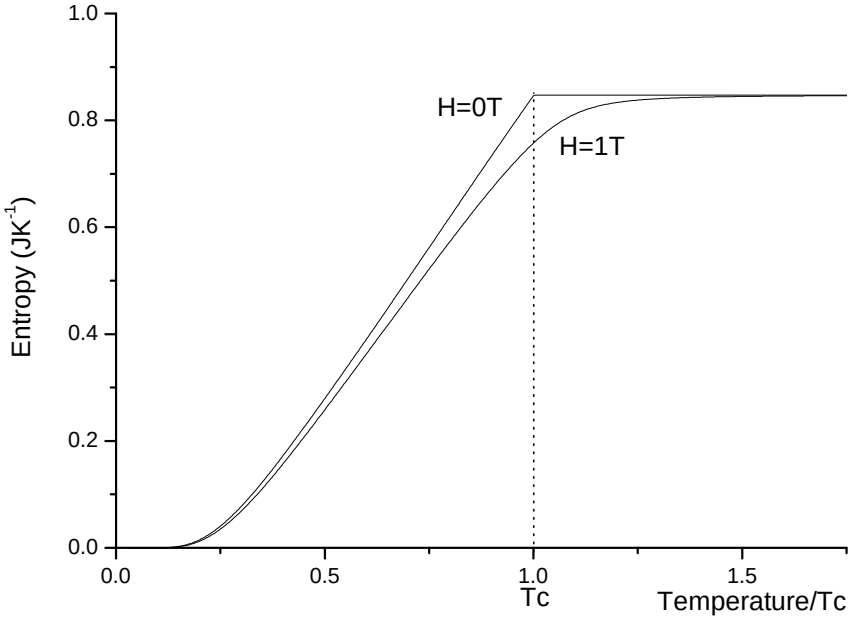

Figure 3.4: Entropy graph for H=0 T and H=1 T, with J=$\frac{3}{2}$ and g=2

in the material behaves like a Paramagnetic one, gradually increasing the entropy variation.

The magnetocaloric effect applied to the construction of a usable refrigerator is all based on the control of this phenomenon of the magnetic entropy change around the Curie temperature.

3.3 Adiabatic Temperature Change

As previously mentioned, the other greatly relevant thermodynamic property for the magnetocaloric effect is the adiabatic temperature change, obtained by considering the entropy as a function of temperature and magnetic field, $S = S(T, H)$, a small element change is represented by:

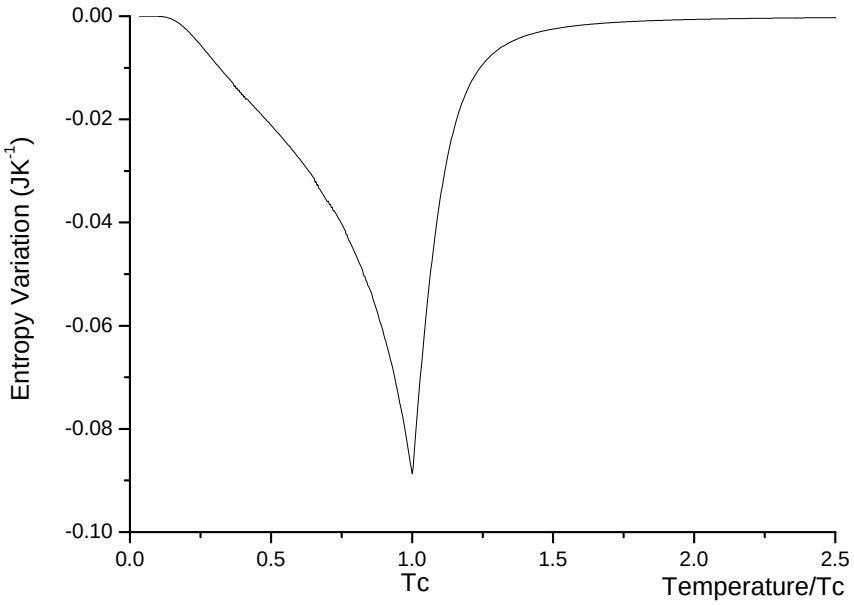

Figure 3.5: Variation of magnetic entropy for a field variation of 0 to 1 T

$$dS = \left(\frac{\partial S}{\partial T}\right)_H dT + \left(\frac{\partial S}{\partial H}\right)_T dT \tag{3.17}$$

Considering an adiabatic process ($dS = 0$) we have the following relation:

$$\left(\frac{\partial S}{\partial T}\right)_H dT = -\left(\frac{\partial S}{\partial H}\right)_T dH \tag{3.18}$$

The specific heat, given by Equation (3.10), connecting with (3.8) and (3.18) we obtain:

$$\frac{C}{T} dT = -\left(\frac{\partial M}{\partial T}\right)_H dH \tag{3.19}$$

and consequently:

$$\Delta T_{ad}(T)_{\Delta H} = \int_{Hi}^{Hf} \left(\frac{T}{C(T,H)}\right)_H \left(\frac{\partial M(T,H)}{\partial T}\right)_H dH \tag{3.20}$$

In this case, one has to take into account the full specific heat of the material, and not only the spin part.

3.4 Relative cooling power

Before advancing to more specific aspects of magnetic cooling we have to first define the relative cooling power (RCP).

This value is one of the most relevant aspects of the analysis of a magnetic material candidate for magnetic cooling and it's very simply defined by the product of the maximum value of the entropy variation by the full width at half maximum (FWHM) of the same entropy variation curve, as such:

$$RCP = \Delta S_{max} FWHM \tag{3.21}$$

expressed in J/kg.

3.5 Thermal magnetic cycles

Taking into account all of the above, it is possible to describe some thermodynamic cycles suitable for the construction of a usable magnetic refrigerator: the Ericsson cycle and the Brayton cycle [13].

3.5.1 Ericsson cycle:

This cycle is based on two isothermal and two isofield processes, following the idea below described:

Step A→B - The magnetic system is without an applied magnetic field. The application of a magnetic field, at constant temperature (isothermal process), will cause an entropy change in the system, and consequently, a heat transportation from the magnetic object to the environment, resulting in a temperature increase in the environment.

Step B→C - At a constant magnetic field, the temperature of the magnetic material is lowered.

Step C→D - The previously applied field is complectly removed resulting in an opposite entropy change, and a heat absorption, from the environment to the magnetic material, decreasing the temperature of the surrounding environment.

Step D→A - Finally the temperature of the magnetic material is risen without applying a field and the cycle is closed.

This cycle is presented in Figure (3.6):

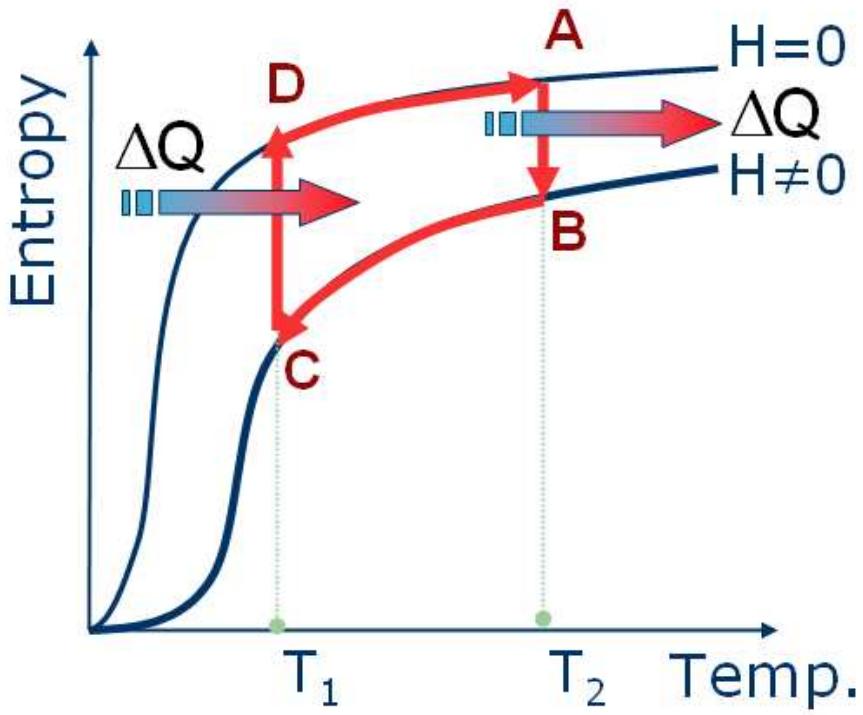

Figure 3.6: Isothermal or Ericsson cycle

3.5.2 Brayton cycle:

This cycle is based on two adiabatic and two isofield processes.

Step A→B - The magnetic material is without applied field. Application of a magnetic field at a constant entropy (adiabatic process), will allow the temperature to vary.

Step B→C - At a constant magnetic field the temperature is reduced, resulting in a variation of entropy and temperature.

Step C→D - Again keeping the entropy constant, we remove the magnetic field, resulting in a temperature decrees.

Step D→A - Finally the temperature is raised until the starting point, again resulting in an increases in temperature.

This cycle is presented in Figure (3.7):

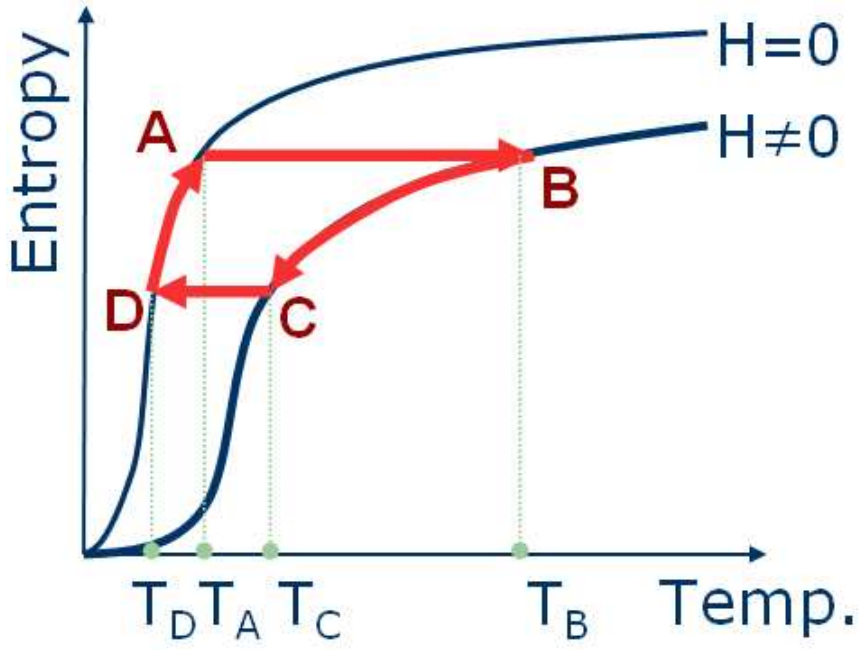

Figure 3.7: Adiabatic or Brayton cycle

Applying the above to a possible practical application we have Figures (3.8) and (3.9) for the Ericsson and Brayton cycles, respectively:

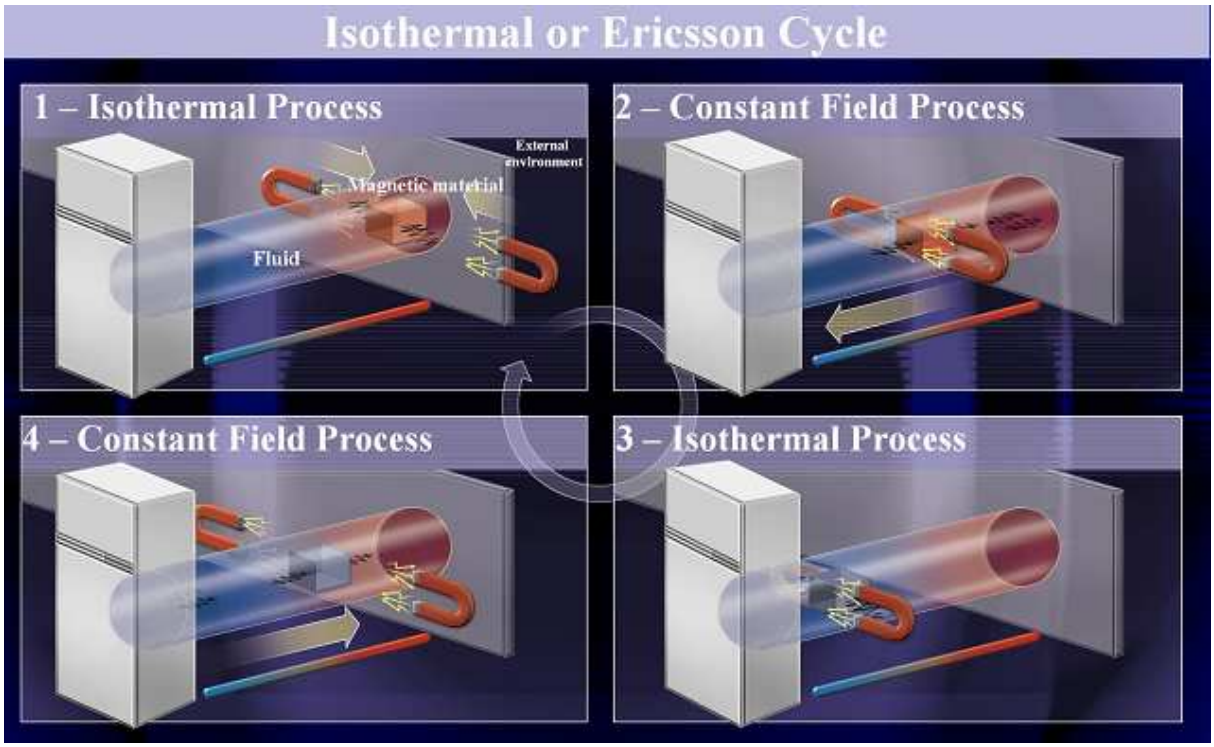

Figure 3.8: Practical Isothermal Cycle Schematics

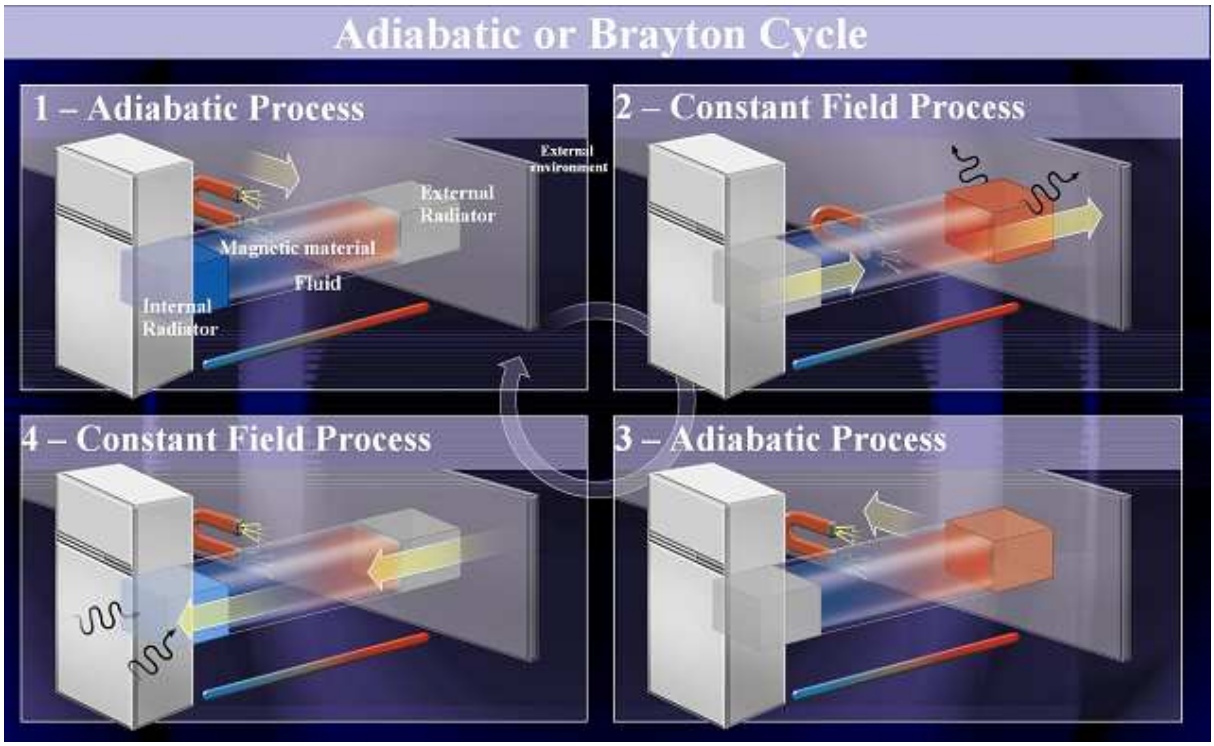

Figure 3.9: Practical Adiabatic Cycle Schematics

Chapter 4

Magnetic materials used in magnetic refrigeration

4.1 Family R-G (R: rare-earths, G: metalloid)

Since the discovery of the huge MCE in $Gd_5Si_2Ge_2$ (35 J/kgK at 280 K), in 1997 [14], extensive study has been done on this alloy. That large ΔS value is due to a coupled magneto-structural first-order transition, driven by temperature [15], magnetic field [16] and pressure [17]. Several series have been studied from this parent compound, namely: (*i*) $Gd_5(Si_{1-x}Ge_x)_4$ alloys, with ΔS ranging from 61 J/kgK at 90 K to 8.6 J/kgK at 340 K [9]; (*ii*) $(Gd,Pr/Tb)_5Si_4$ [18], without any significant change on the magnetocaloric properties; (*iii*) $R_5(Si_{1-x}Ge_x)_4$ alloys, where R means a rare-earth, like Nd [19], Tb [20], Dy [21] and Ho [22]; and (*iv*) many others [9]. Also interest is the work of Morellon et al [17] that could merge the structural and magnetic transition of $Tb_5Si_2Ge_2$ compounds by applying 8.6 kbar of hydrostatic pressure; increasing therefore the MCE.

4.2 Family R-M-G (M: transition metal)

Another series with magneto-structural coupling is the $La(Fe_xSi_{1-x})_{13}$ [23]. For instance, ΔS for x=0.88 reaches 26 J/kgK at 188 K. These compounds under a negative pressure (expansion of the unit cell), via insertion of Hydrogen, could shift the transition temperature up to RT [24]; on the other hand, positive pressure (compression of the unit cell), via hydrostatic pressure, increases the ΔS value, decreasing, however, the transition temperature [25]. Substitution of 50% of Pr for La has also been done [26], increasing the value of ΔS for 30 J/kgK at 185 K .

4.3 Family Mn-M-G

MnAs is a compound that presents a coupled magneto-structural first order transition, resulting therefore in a huge ΔS: 32 J/kgK at 318 K [27]. Wada et al. [27], studied Mn(As,Sb) and found that both, transition temperature and ΔS decrease by adding Sb; disregarding therefore this series comparing to the parent compound. More recently, Gama et al. [28] applied 2.2 kbar in MnAs compound and could increase the ΔS up to 267 J/kgK at 280 K. Other compounds with Mn are those of the series MnFe(P,As). Tegus et al. [29] pointed out the highest ΔS value of that series: 32 J/kgK at 220 K for the compound $MnFeP_{0.65}As_{0.35}$.

Concerning the Heusler alloys Ni_2MnGa, this material has a decoupled magneto-structural transition of about 100 K. Hu et al. [30] was the first to report the magnetocaloric properties of this compound, and, more recently, Zhou et al. [31] reported a coupled magneto-structural transition for the out of stoichiometry $Ni_{55}Mn_{19}Ga_{26}$, with a

huge, but narrow, ΔS: 20 J/kgK at 317 K.

4.4 Manganites family ($RMnO_3$)

The MCE of mixed-valency manganites was first measured by Morelli et al. in 1996, for thick films of $La_{2/3}(Ca/Sr/Ba)_{1/3}MnO_3$ [32]. The magneto-structural coupling [33] and the numerous possibilities of exchanging elements in synthesis make manganites a rich field in MCE study.

The substitution of La by other rare-earth ion in $La_{2/3}Ca_{1/3}MnO_3$ or $La_{2/3}Sr_{1/3}MnO_3$ manganite can tune the transition temperature and enhance magnetocaloric properties [34]. Some manganites systems show also a magneto-structural coupling, due to charge/orbital ordering [9, 35]. For instance, Chen and co-workers found a ΔS value of 7.1 J/kg.K near the charge/orbital ordering temperature (161 K) of the $Pr_{0.5}Sr_{0.5}MnO_3$ manganite [36].

4.5 Intermetallics family R-M

There are several sub-families, namely the Laves Phase compounds, as RCo_2 [37], RAl_2 [38] and RNi_2 [39], but all of these are not suitable for applications around room temperature due to their low values of ΔS and T_c. On the contrary, those systems are the reason of several theoretical models, due to its interesting, from the academic point of view, magnetocaloric properties [39]. Other compounds can also be cited: Nd_2Fe_{17} (5.9 J/kgK at 325 K) [40], Gd_7Pd_3 (6.5 J/kgK at 323 K) [41], Gd_4Bi_3 (2.7 J/kgK at 332 K) [42] and Gd_2In (4.5 J/kgK at 194 K) [43].

All of those values of ΔS above reported are related to 5 T of magnetic field change.

All of those families above described, and their corresponding compounds, have problems that avoid their immediate application in a magnetic cooling device. We can mention those systems with (*i*)first order magnetic transition and a consequent thermal hysteresis, producing therefore energy losses during the thermo-magnetic cycle; (*ii*) high pure rare-earth metals, making them economically unviable; (*iii*) elements that need special handling, for instance the poisonous Arsenic; (*iv*) narrow ΔS curve, avoiding therefore a wide thermo-magnetic cycle and, finally, (*v*) low values of ΔS, decreasing the cooling power of the device.

4.6 The studied Ni_2Mn(Ga,Bi) alloy

The Ni_2MnGa alloy is widely studied due to both its particular magnetic properties and as a shape memory alloy, with a cubic-like structure. In addition to the magnetic transition at T_c it also undergoes a martensitic to austenitic transition at a temperature T_M; a transition that is also associated to an entropy variation. [30, 44–46].

The study of this alloy has also shown that the partial substitution of Ni for Mn results in an increase of T_M and a decrees of T_c [47–49]. The study of $Ni_{2+x}Mn_{1-x}Ga$ alloy has shown that these two temperatures merge at a composition range of $0{,}18 \leq x \leq 0{,}2$ [50–52], resulting in a great entropy change around the $T_M = T_c$ temperature. This result was called the giant magnetocaloric effect (GMCE).

Also the alloying of Ni_2MnGa with several elements has proven to also couple the two transitions. Cu, for instance, in the composition $Ni_2Mn_{0.75}Cu_{0.25}Ga$ has achieved this result at a T_c=T_M=RT [53, 54]

An interesting study by Söderberg *et al* [55] has shown the results of a fourth element addition in the alloy Ni_2MnGa. Although the objective of the referred paper was only to study the variation of the transition temperatures, among the various elements added to the alloy an addition of 2% Bi has shown to also increases T_M and decrees T_c. As such, the objective of the current work is the study of a series of Ni_2MnGa_{1-x},Bi_x quaternary alloys, with $0 \leq x \leq 0{,}5$, to see if T_M and T_c merge is possible in a usable temperature for magnetic refrigeration.

Chapter 5

Experimental Procedure

5.1 Sample Preparation

Usually such intermetallic compounds are prepared by melting. The $Ni_2Mn(Ga_{1-x},Bi_x)$ alloys were prepared in a Buhler arc melting furnace, at the University of Porto, with the appropriate amount of constituent elements. The furnace works with a water-cooled copper crucible was pre-evacuated better than 2×10^{-6} mbar and refilled with high-purity argon gas. The samples were arc melted three times, as to obtain homogeneous samples, and also, a titanium piece was melted inside the furnace as an oxygen trap. The materials used in the preparation of the various alloys are stated in table (5.1).

Table 5.1: Materials used in the $Ni_2Mn(Ga_{1-x}, Bi_x)$ samples

Material	Alpha Aesar Code	Purity	From
Nickel	42332	99,99%	slug
Manganese	36221	99,98%	irregular pieces
Gallium	10185	99,9999%	ingot
Bismuth	14442	99,999%	polycrystalline lump

In order to create homogeneous alloys, the samples were subjected to heat treatment. The samples were sealed in evacuated quartz tubes and annealed at 1073 K for eleven days and then quenched in liquid nitrogen, following the literature directions [48].

The author of this report did not participate in the preparation of these samples.

5.2 Characterization

5.2.1 1º - X-ray diffraction

This analysis was performed at the University de Trás-os-Montes e Alto Douro (UTAD) using a multichannel x-ray diffractometer with a Cu and Ka_{α} radiation. By doing so it is possible to detect both the main phase and the impurity phases, as long as these later ones are present in quantities of at least 5 vol %. Then, using the refinement procedure of the software PowderCell [1] the crystal structure and lattice parameters were analyzed.

The author of this report did not participate in these measurements, only in their analysis.

5.2.2 2º - Energy dispersive x-ray spectroscopy EDS

In order to check the homogeneity and stoichiometry of the samples, an EDS/SEM was used, more precisely the Phillips-FEI/Quanta 400, from the University of Trás-os-Montes e Alto Douro. To achieve a more reliable result, up to six measurements were performed on each sample. These results can be obtained within 5% of certainty.

[1] $http://users.omskreg.ru/\ kolosov/bam/a_v/v_1/powder/e_cell.html$

The author of this report did not participate in these measurements, only in their analysis.

5.2.3 3º - Magnetic measurements

The magnetic measurements M(T,H) were performed with a vibrating sample magnetometer (VSM) at the University of Aveiro, with a temperature range from 2 to 300 K and a field range from 0 to 10 T, and at the University of Porto, with a temperature range from 300 to 1000 K and a field range from 0 to 1 T. A field strength of 1 T was used because this is a feasible field to be created by a permanent magnet in a magnetic refrigerator.

From the many information available in a VSM measurement, we focus mainly in the T_c and T_M determination, both of which observable in a representation of magnetization versus temperature we also measure the isothermal curve of magnetization, observable as a magnetization versus field strength for different temperatures to determine therefore the magnetic entropy change.

Chapter 6

Results and Discussion

6.1 X-ray diffraction

After the X-ray diffraction analysis we concluded that, from the six $Ni_2Mn(Ga_{1-x},Bi_x)$ compositions (x=0;0,1;0,2;0,3;0,4;0,5), only the sample with x=0, Ni_2MnGa, did not present a secondary phase, all others were not single phase materials, as intended.

The list of found phases can be observed in table (6.1)

Table 6.1: $Ni_2Mn(Ga_{1-x},Bi_x)$ samples phases

Phases	x=0	x=0,1	x=0,2	x=0,3	x=0,4	x=0,5
Ni_2MnGa	present	present	present	not present	not present	not present
Bi	not present	present	present	present	present	present
Mn	not present	present	present	?	?	?
Ga_3Ni_5	not present	not present	not present	present	present	present
Bi_3Ni	not present	not present	not present	present	present	present

Results showing the same phases can be observed in the X-ray refinement images in Appendix C, for all the samples produced.

6.2 Energy dispersive X-ray spectroscopy EDS

The EDS technique indicates deviations that are less than 5% when compared with the nominal atomic percentage for each sample. It is still important to note that the composition variation of the analysis is sometimes within this value.

So, the EDS results show that the approach to the studied alloy was not the appropriate. Clear evidence of this can be seen in images (D.1) to (D.6), produced by scanning electron microscope (SEM) in Appendix D.

Analyzing the SEM photos we can see, in Figure (D.1), corresponding to the composition Ni_2MnGa, that there doesn't seem to be any evidence of secondary phases or unmixed materials. In Figure (D.2), corresponding to the composition $Ni_2MnGa_{0,9}Bi_{0,1}$, small white spots are visible, possibly evidencing the occurrence of a bismuth secondary phase during thermic treatment. In Figure (D.3), corresponding to the composition $Ni_2MnGa_{0,8}Bi_{0,2}$, different bright and a dark areas are visible. Figures (D.4) and (D.5), corresponding to the compositions $Ni_2MnGa_{0,7}Bi_{0,3}$ and $Ni_2MnGa_{0,6}Bi_{0,4}$, both show bright and dark areas as well as white spots. Figure (D.6), corresponding to the composition $Ni_2MnGa_{0,5}Bi_{0,5}$, show two very different dark and bright areas.

The following table, (6.2) presents the data from the EDS for each sample.

Table 6.2: EDS results

(a) Ni_2MnGa				
	Ni at %	Mn at %	Ga at %	Bi at %
Nominal	50	25	25	0
EDS	50,4	24,8	24,8	0
(b) $Ni_2MnGa_{0,9}Bi_{0,1}$				
	Ni at %	Mn at %	Ga at %	Bi at %
Nominal	50	25	22,5	2,5
EDS	51	25.4	22,7	0,8
(c) $Ni_2MnGa_{0,8}Bi_{0,2}$				
	Ni at %	Mn at %	Ga at %	Bi at %
Nominal	50	25	22,5	2,5
EDS	51	25.4	22,7	0,8
(d) $Ni_2MnGa_{0,7}Bi_{0,3}$				
	Ni at %	Mn at %	Ga at %	Bi at %
Nominal	50	25	17,5	7,5
Region 1 (bright)	10,39	4,06	1,98	83,57
Region 2 (dark)	46,49	22,38	28,41	2,71
(e) $Ni_2MnGa_{0,6}Bi_{0,4}$				
	Ni at %	Mn at %	Ga at %	Bi at %
Nominal	50	25	15	10
Region 1 (bright)	10,94	5,02	1,5	82,54
Region 2 (dark)	49,34	24,52	21,31	4,83
(f) $Ni_2MnGa_{0,5}Bi_{0,5}$				
	Ni at %	Mn at %	Ga at %	Bi at %
Nominal	50	25	12,5	12,5
Region 1 (bright)	11,78	2,29	0	85,94
Region 2 (dark)	7,02	54,19	2,31	36,48
Region 3 (waves)	62,39	24,67	12,28	0,66

Table (6.2(a)), for Ni_2MnGa, was made with the average of six measurements, showing a good agreement with the nominal composition for this sample. Others, like for example $Ni_2MnGa_{0,9}Bi_{0,1}$, table (6.2(b)), show a clear deviation from the nominal composition. Samples like $Ni_2MnGa_{0,8}Bi_{0,2}$, table (6.2(c)), or $Ni_2MnGa_{0,7}Bi_{0,3}$, table (6.2(d)), that present clearly different regions, also show a different composition in these regions.

The causes for such results in the bismuth alloyed samples could be various. The images suggest the occurrence of a liquid phase, this could be due to the presence of unalloyed bismuth, that has a melting temperature of 545 K, lower than the temperature of the heat treatment. Although Söderberg [55] did not mention any difficulties in his work, the amount of alloying element (Bi) was only 2%, being our minimum ($Ni_2MnGa_{0,9}Bi_{0,1}$) 10%. Knowing this it is possible that we broke the solubility limit for (Bi) in the first sample, causing all these unwanted results.

6.3 Magnetic measurements

Since only the sample with composition Ni_2MnGa, with no bismuth alloying, had a pure phase and a homogeneous composition, valid magnetic measurements can only be performed on this sample.

A total of eight measurements where performed on the sample. Measurements for: A - increasing field and increasing temperature; B - decreasing field and increasing temperature; C - increasing field and decreasing temperature; D - decreasing field and decreasing temperature; all of which for above and below room temperature.

The above room temperature measurements where performed in the University of Porto and the below room temperature in the University of Aveiro.

First of all we performed a measurement of Magnetization as a function of temperature for small field, for below and above room temperature, presented in Figure (6.1).

It can be observed that the measurements, above and below RT do not match at 300K. This may be due to several factors, for instance the previous magnetic history of the

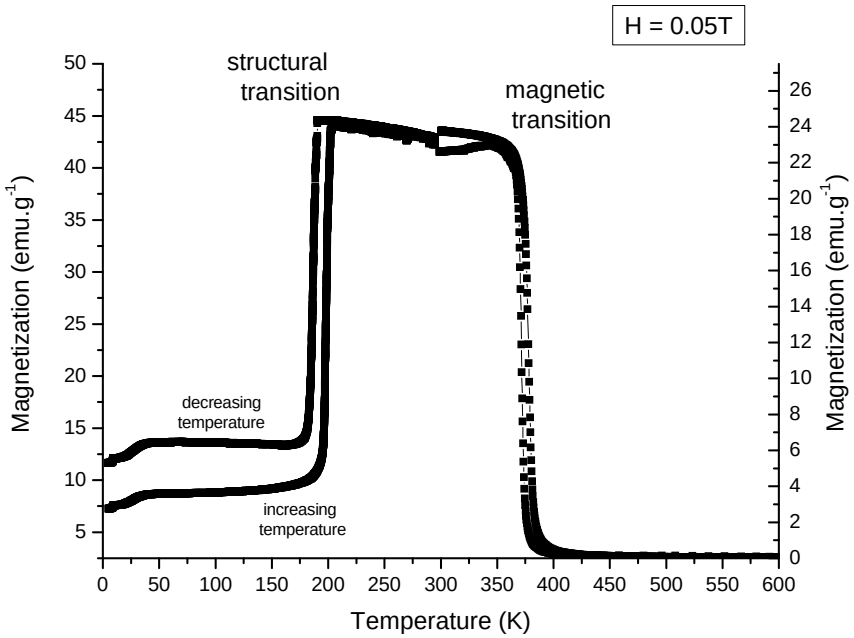

Figure 6.1: Magnetization measurement for small magnetic field

sample, the demagnetization factor, that has been determined to be 6.23 emu.g^{-1}/T and 22 emu.g^{-1}/T for the samples used in the below and above RT measurements respectively, domain walls, etc.

Also, the sample used for the below RT measurements was heated above T_c as to cancel the sample's thermal history, previously to the measurements. In the sample used for the above RT measurements this factor was not taken into consideration, however, since the magnetization was first measured with increasing temperature, once T_c was crossed the thermal history was erased, and in the following decreasing temperature measurement there was no thermal history.

For the measurements for below room temperature we found that the martensitic transition (decreasing temperature), occurs at T_M=186 K and the austenitic transition (increasing temperature), at T_M=197 K. This originates a hysteresis of about 11 K. Such a hysteresis is naturally present in first order transitions and structural transition, being

both the case in this specific transition. These values for T_M are in accordance with previous literature data [9, 46].

For the measurements for above room temperature, the hysteresis around the magnetic transition temperature T_c between increasing and decreasing temperature is almost unnoticeable having a value of about T_c=375 K. This value is in accordance with previous literature data [9, 56].

We then measured the magnetization for field variation, for T=5 K and a variation of field from 0 to 10 T, presented by Figure (6.2).

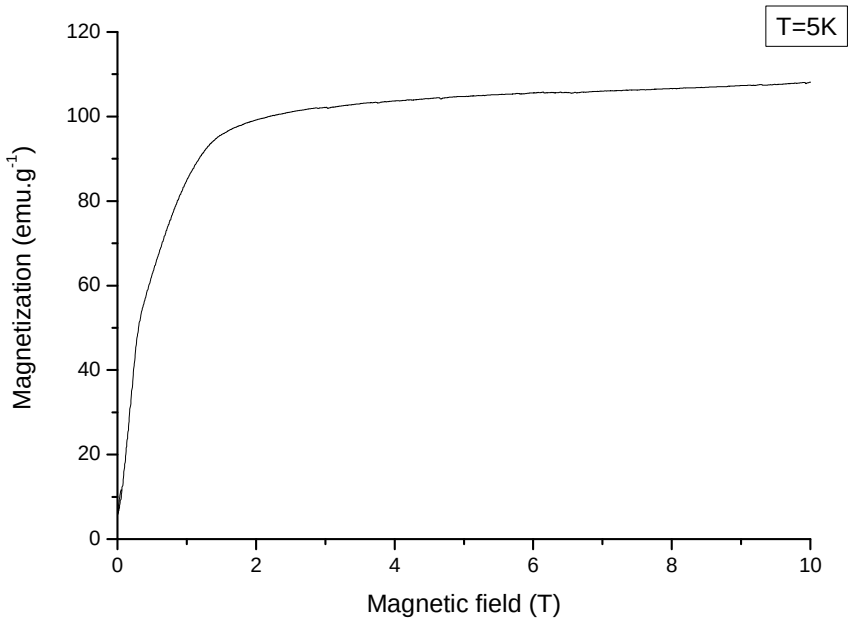

Figure 6.2: Magnetization in order of magnetic field for 5K from 0 to 10 T

In Figure (6.2) we can measure the saturation magnetization. This value is approximately 105 emu.g^{-1} about 4.55 μ_B/FU[1], in good accordance with previous literature [56, 57].

We also measured the magnetization as a function of the magnetic field for T=150 K

[1]FU=funtional units

and T=250 K, below and above the structural transition temperature T_M respectively, presented in Figure (6.3(a)), and in detail in Figure (6.3(b))

Once again, as in the low temperature magnetization measurements, we clearly notice a hysteresis between the rising field and lowering field for the T=150 K measurement, below the structural transition temperature, while in the measurement for T=250 K such a hysteresis is nearly undetectable, the saturation magnetization in these measurements is, for T=150K, 104 emu.g^{-1} about 4.51 μ_B/FU and for T=250K, 90 emu.g^{-1} about 3.9 μ_B/FU. Also we notice a clear difference between the saturation value of the magnetization above and below the structural transition.

For the calculation of the entropy variations we measured the magnetization as a function of magnetic field for both below and above room temperature, presented in Figures (6.4) and (6.5) respectively.

Figure (6.4) has been produced without the demagnetization field correction and Figure (6.5) with the correction, revealing the influence this factor has on magnetic measurements.

From the measurements of magnetization as a function magnetic field we determine the variation of magnetization with temperature; for below room temperature Figure (6.6) and for above room temperature Figure (6.7).

Two completely different processes are illustrated in these Figures. Figure (6.6), refers to the magnetization variation due to the structural martensitic-austenitic transition around T_M and Figure (6.7) refers to the Ferromagnetic-Paramagnetic transition due to electron spin misalignment around T_c.

From this, and using Eq. (3.9), we can finally calculate the entropy variation for these

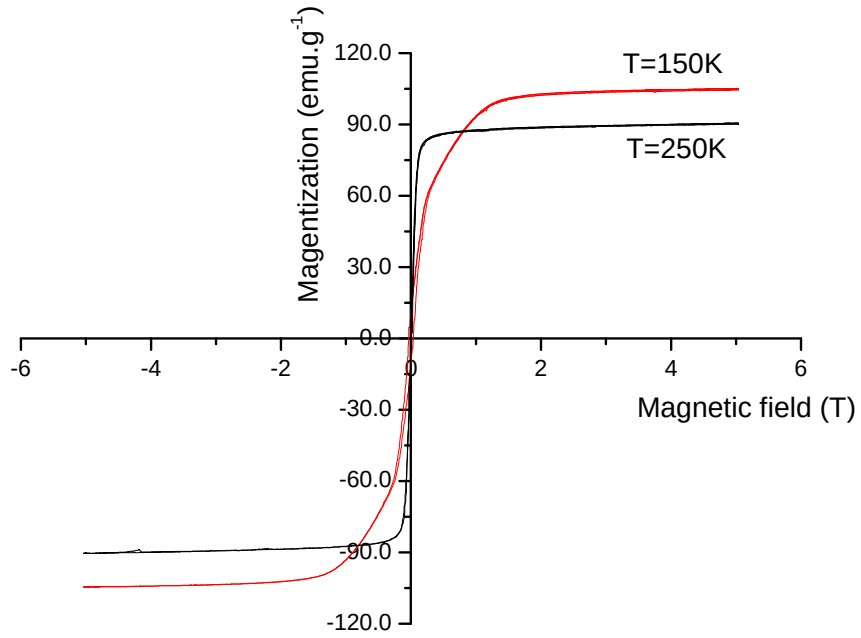

(a) Magnetization variation as a function of magnetic field for 150 K and 250 K (below and above the structural transition temperature)

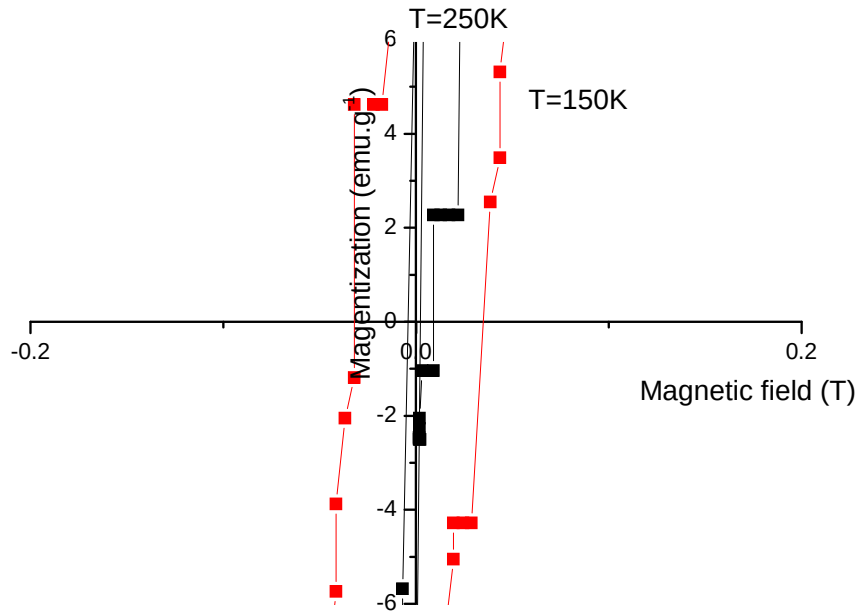

(b) Magnetization variation as a function of magnetic field for 150 K and 250 K in detail

Figure 6.3: Magnetization variation as a function of magnetic field at 150 K and 250 K

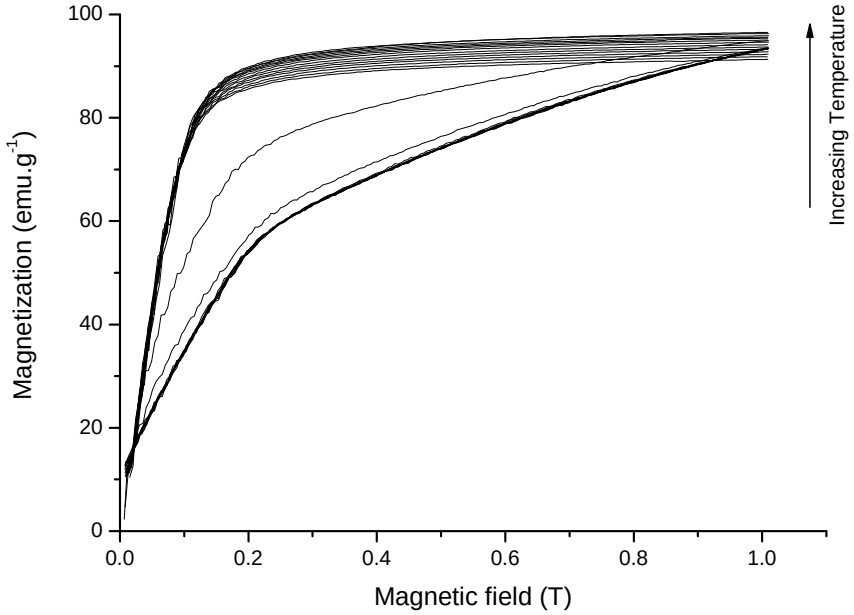

Figure 6.4: Magnetization in order of magnetic field for below room temperature (increasing temperature, increasing field) between 175 and 205 K

measurements.

6.3.1 Magnetic entropy results

The magnetic entropy change in measurements A (increasing field and increasing temperature), B (decreasing field and increasing temperature), C (increasing field and decreasing temperature), and D (decreasing field and decreasing temperature), related to the magnetic transition, around T_c, revealed the following maximum results at a magnetic field change ΔH=1T: ΔS^A_{max}=-1.25 Jkg^{-1}K^{-1} and T_c=384 K, ΔS^B_{max}=-1.3 Jkg^{-1}K^{-1} and T_c=383 K, ΔS^C_{max}=-1.3 Jkg^{-1}K^{-1} and T_c=386 K and ΔS^D_{max}=-1.3 Jkg^{-1}K^{-1} and T_c=387 K.

As for measurements A, B, C and D, related to the structural transition, around T_M, these revealed the following maximum values: ΔS^A_{max}=4.6 Jkg^{-1}K^{-1} and T_M=197 K, ΔS^B_{max}=4.45 Jkg^{-1}K^{-1} and T_M=196.4 K, ΔS^C_{max}=4.7 Jkg^{-1}K^{-1} and T_M=190.3 K and

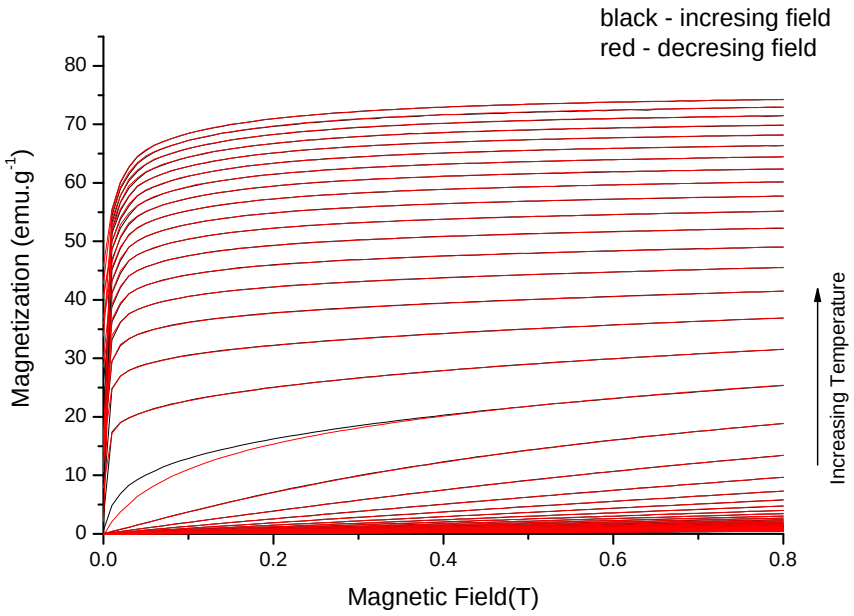

Figure 6.5: Magnetization as a function of magnetic field for above room temperature (increasing temperature, increasing and decreasing field) between 300 and 620 K

ΔS^{D}_{max}=5 $Jkg^{-1}K^{-1}$ and T_M=189.4 K.

Figure (6.8) shows all entropy variation measurements, Figure (6.9(a)) and (6.9(b)) show the entropy variation peaks in detail, using the Origin B-Spline function to interpolate the experimental data. Table (6.3) summarizes all the above information plus the FWHM for each measurement and correspondent RCP:

Table 6.3: Summary of all the entropy variation curve information, including the FWHM and correspondent RCP

	Trans. type	Trans. temp.(K)	Δ S_{max}($Jkg^{-1}K^{-1}$)	FWHM(K)	RCP(J/Kg)
Measurement A	magnetic	384	-1.25	29	36.25
Measurement B	magnetic	383	-1.3	28	36.4
Measurement C	magnetic	386	-1.3	27.5	35.75
Measurement D	magnetic	387	-1.3	28	36.4
Measurement A	structural	197.0	4.6	4	18.4
Measurement B	structural	196.4	4.45	3.5	15.6
Measurement C	structural	190.3	4.7	4	18.8
Measurement D	structural	189.4	5	3.9	19.5

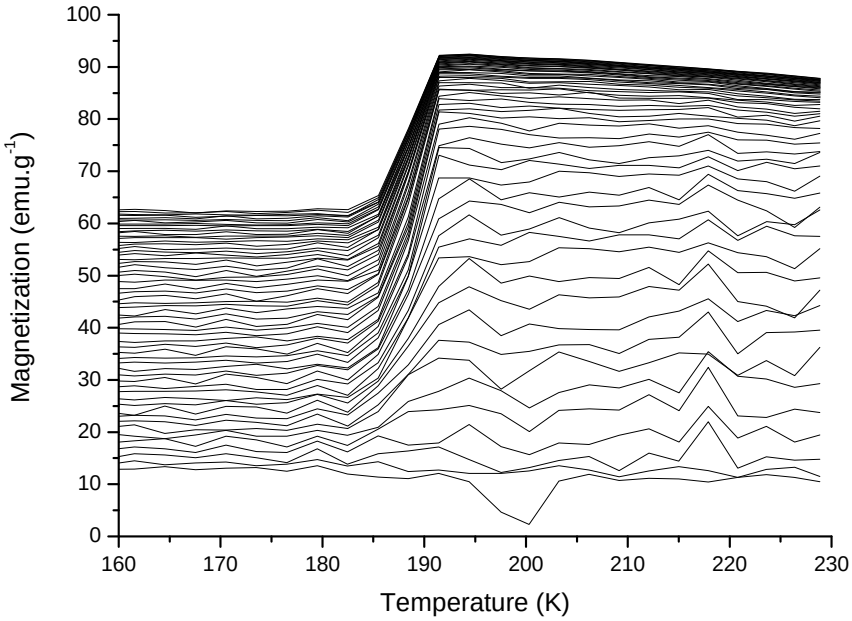

Figure 6.6: Magnetization as a function of temperature for below room temperature (decreasing temperature, decreasing field), from 0 to 1 T

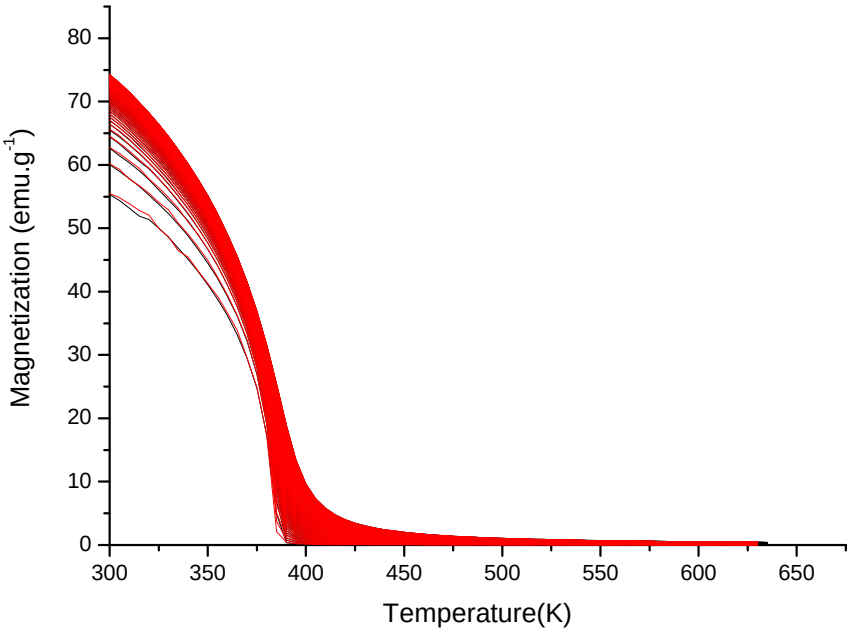

Figure 6.7: Magnetization as a function of temperature for above room temperature(increasing temperature, increasing and decreasing field), from 0 to 1 T

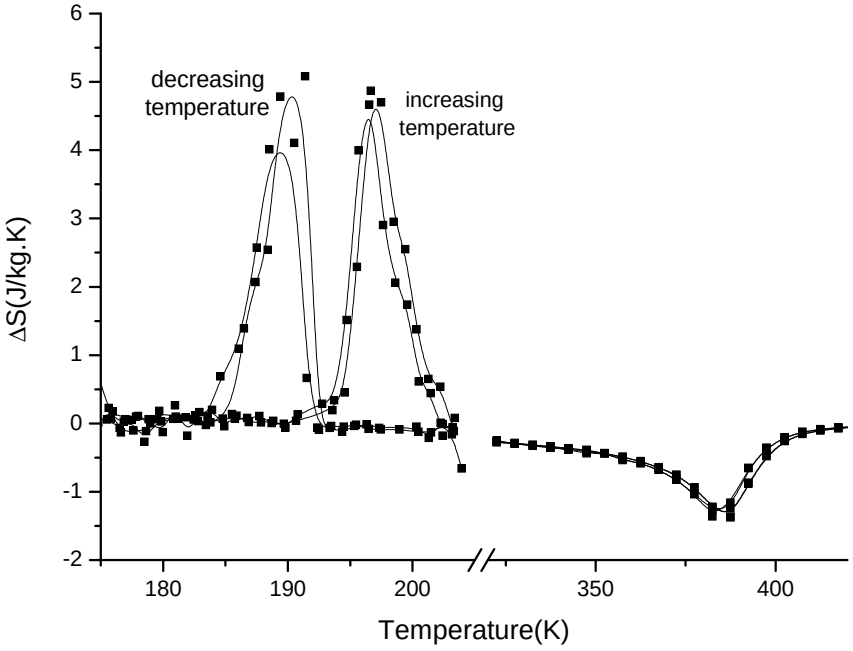

Figure 6.8: Entropy variation for all measurements, with ΔH=1T

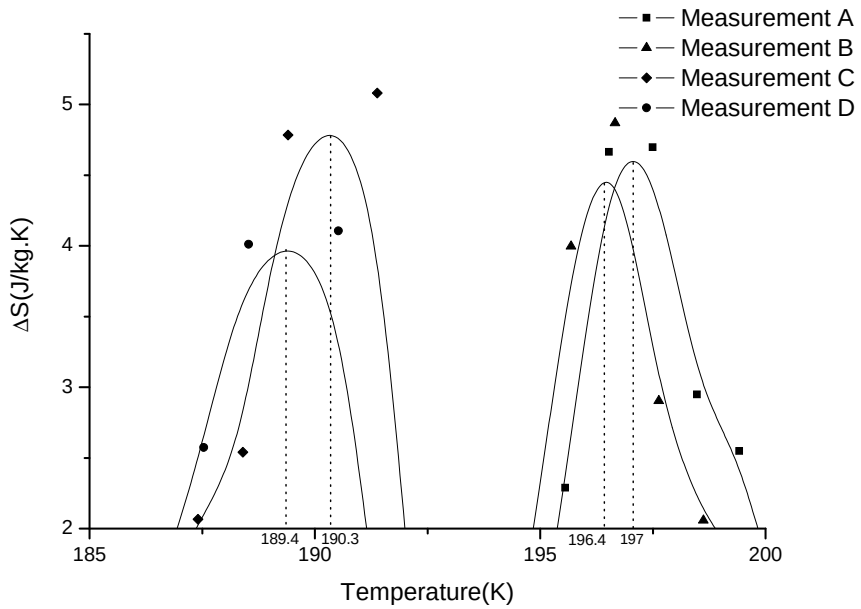

(a) Detail on the peaks of the entropy variation for below room temperature measurements A, B, C and D

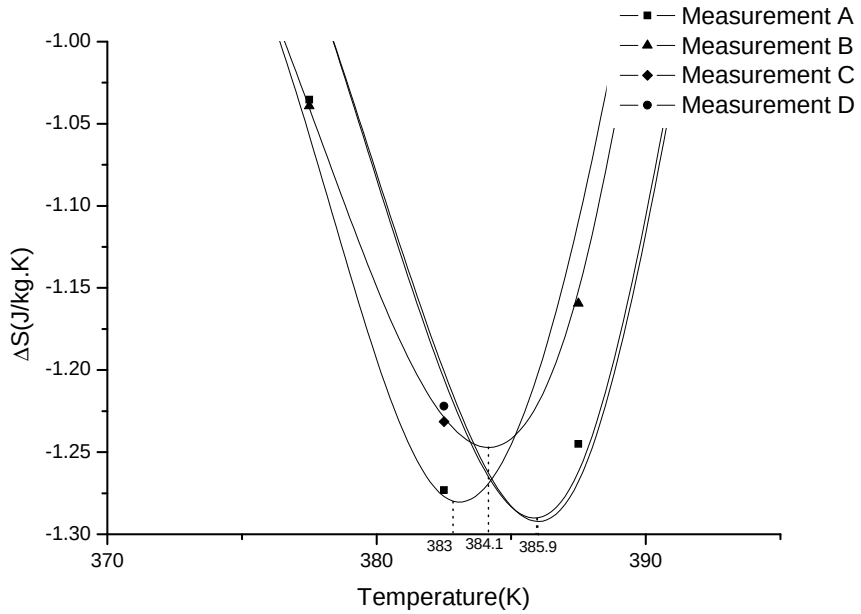

(b) Detail on the peaks of entropy variation for above room temperature measurements A, B, C and D

Figure 6.9: Detail on the entropy variation peaks

Chapter 7

Conclusions

The objective of this work was the study of the magnetocaloric effect of the Heusler alloy Ni_2MnGa with bismuth alloying, in a search for a stoichiometry where the magnetic and structural transitions would merge and create a giant magnetocaloric effect. This was not possible due to the fact that all the alloyed samples presented a secondary phase, becoming useless for our study.

However the seed sample, Ni_2MnGa, was produced with great success and allowed the study of MCE properties. All its measurements, as its entropy variations of ΔS=4.7 $Jkg^{-1}K^{-1}$ for the structural transition and ΔS=-1.29 $Jkg^{-1}K^{-1}$ for the magnetic transition, are in agreement with previous literature data [30,31,45–47,58], as was its suturation magnetization of 4.55 μ_B/FU [56, 57]

Chapter 8

Future work

Since only one pure sample was produced, Ni_2MnGa (x=0), the straight-forward future work is the study of bismuth's solubility limit and a new set of $Ni_2Mn(Ga_{1-x},Bi_x)$ alloys, this time with a much smaller concentration of bismuth, a study indeed initiated with already melted samples.

If all goes correctly we will be able to reproduce the results obtained by Söderberg [55], approximating T_c and T_M and possibly merging them, creating the giant magnetocaloric effect.

Apêndice A

Magnetization expression development

As developed in the book "Magnetism and Magnetic Resonance in Solids" by Guimarães and Oliveira [10] we have the following:

$$M = g\mu_B \frac{\sum_{m_J} m_J \exp(g\mu_B B m_J / k_B T)}{\sum_{m_J} \exp(g\mu_B B m_J / k_B)} \tag{A.1}$$

considering

$$x = \frac{g\mu_B JB}{k_B T} \tag{A.2}$$

and

$$v = \sum_{m_J} \exp\left(\frac{x m_J}{J}\right) \tag{A.3}$$

(partition function)

We have that:

$$M = g\mu_B J \frac{\sum_{m_J}(m_J/J)\exp(xm_J/J)}{\sum_{m_J}\exp(xm_J/J)} = g\mu_B J \frac{dv/dx}{v} \tag{A.4}$$

Being that v is the sum of terms of a geometric progression. Making $z = \exp(x/J)$, we have:

$$v = \sum_{m_J=-J}^{J} z^{m_J} = z^{-J}(1 + z + z^2 + ... + z^{2J}) \tag{A.5}$$

(since $m_J = -J, -J+1, ..., +J$)

Knowing that

$$S_n = a_0 + a_0^2 + ... + a_0^{n-1} = \frac{a_0(x^n - 1)}{x - 1} \tag{A.6}$$

we obtain

$$v = z^{-J}\frac{z^{2J+1} - 1}{z - 1} = \frac{z^{J+1/2} - z^{-(J+1/2)}}{z^{1/2} - z^{-1/2}} \tag{A.7}$$

being

$$z^{J+1/2} = \left(\exp\left(\frac{x}{J}\right)\right)^{J+1/2} = \exp\left(x + \frac{x}{2J}\right) \tag{A.8}$$

$$v = \frac{\exp[(1 + 1/2J)x] - \exp[-(1 + 1/2J)x]}{\exp(x/2J) - \exp(-x/2J)} \tag{A.9}$$

but since $\sinh(x) = [\exp(x) - \exp(-x)]/2$, we can write:

$$v = \frac{\sinh(1+1/2J)x}{\sinh(x/2J)} \tag{A.10}$$

resolving the derivative of v, we obtain:

$$\frac{dv}{dx} = \frac{\sinh(x/2J)(1+1/2J)\cosh[(1+1/2J)x]}{[\sinh(x/2J)]^2} - \frac{\sinh[(1+1/2J)x](1/2J)\cosh(x/2J)}{[\sinh(x/2J)]^2} \tag{A.11}$$

applying to equation (A.4) we have:

$$M = g\mu_B J \frac{dv/dx}{v} = g\mu_B J \left[\frac{(1+1/2J)\cosh[(1+1/2J)x]}{\sinh[(1+1/2J)x]} - \frac{(1/2J)\cosh(x/2J)}{\sinh(x/2J)} \right] \tag{A.12}$$

or

$$M = g\mu_B J \left[\left(1+\frac{1}{2J}\right)\cosh\left[\left(1+\frac{1}{2J}\right)x\right] - \frac{1}{2J}\cosh\left(\frac{x}{2J}\right)\right] \tag{A.13}$$

and finally:

$$M = g\mu_B J B_J(x) \tag{A.14}$$

Apêndice B

Spin entropy change expression development

$$S = -k_B \sum_{m_J} P_{m_J} \ln P_{m_J} \tag{B.1}$$

where

$$P_{m_J} = \frac{\exp(g\mu_B m_J H/k_B T)}{\sum_{m_J} \exp(g\mu_B m_J H/k_B T)} \tag{B.2}$$

We then have:

$$\frac{S}{k_B} = -\frac{\sum_{m_J} \exp(g\mu_B m_J H/k_B T)}{\sum_{m_J} \exp(g\mu_B m_J H/k_B T)} \ln\left(\frac{\exp(g\mu_B m_J H/k_B T)}{\sum_{m_J} \exp(g\mu_B m_J H/k_B T)}\right) \tag{B.3}$$

From equations (A.2) and (A.3) we then have:

$$\frac{S}{k_B} = -\frac{1}{v}\left(\sum_{m_J} \exp(xm_J/J)(\ln\exp(xm_J/J) - \ln v\right) \tag{B.4}$$

$$\frac{S}{k_B} = -\frac{1}{v}\left(\sum_{m_J} \exp(xm_J/J)xm_J/J - \sum_{m_J} \exp(xm_J/J)\ln v\right) \tag{B.5}$$

again, from equation (A.3) we have:

$$\frac{S}{k_B} = -xv\frac{m_J}{J} - \frac{v}{v}\ln v \tag{B.6}$$

from the full development in Appendix A we find:

$$= \ln v - xB_J \tag{B.7}$$

and from equation (A.10) finally

$$S = \ln\left(\frac{\sinh\left[x\left(1+\frac{1}{2J}\right)\right]}{\sinh\left[\frac{x}{2J}\right]}\right) - xB_J(x) \tag{B.8}$$

Apêndice C

X-ray diffraction for

$Ni_2Mn(Ga_{1-x}, Bi_x)$

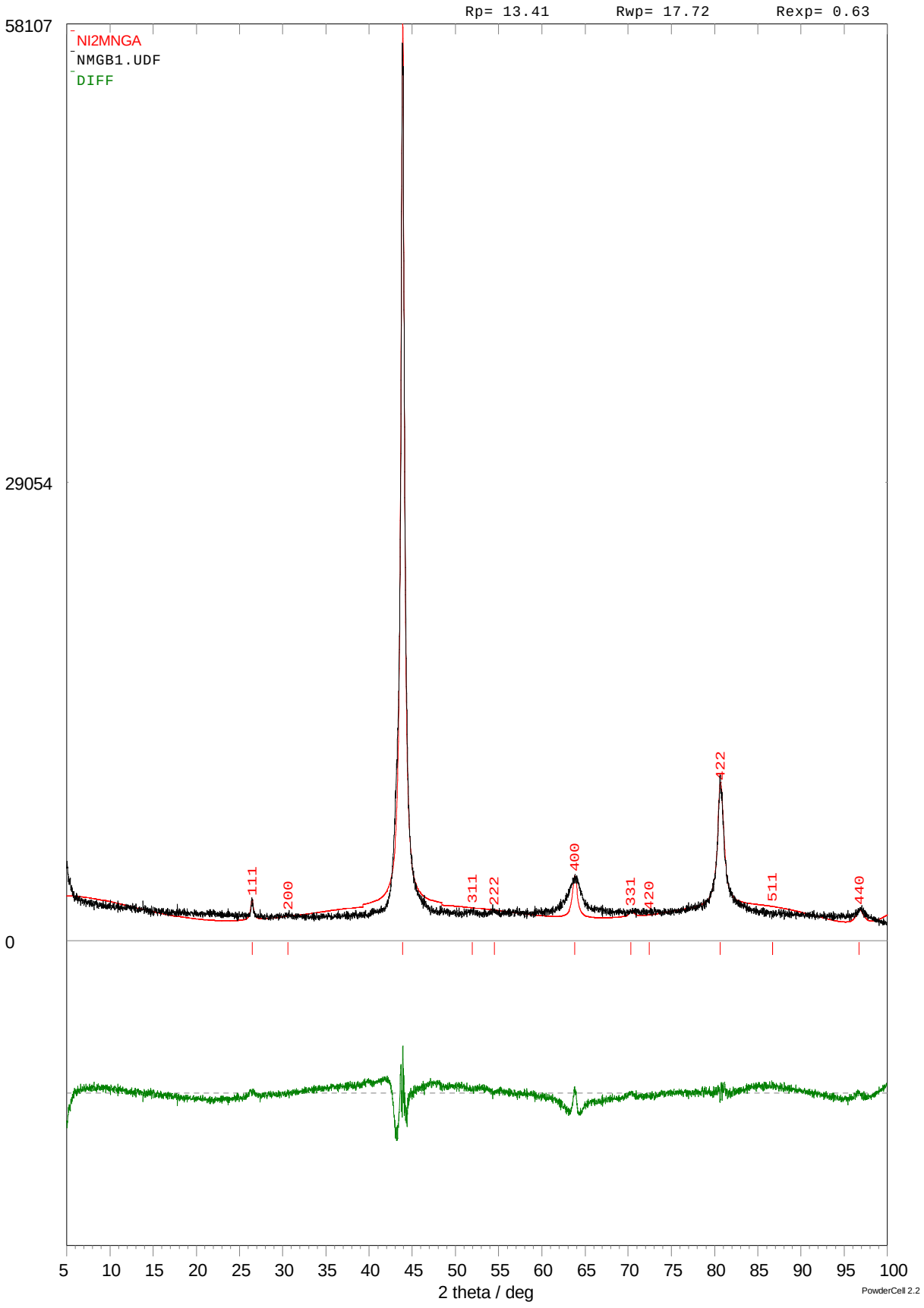

Figure C.1: X-ray diffraction for Ni_2MnGa

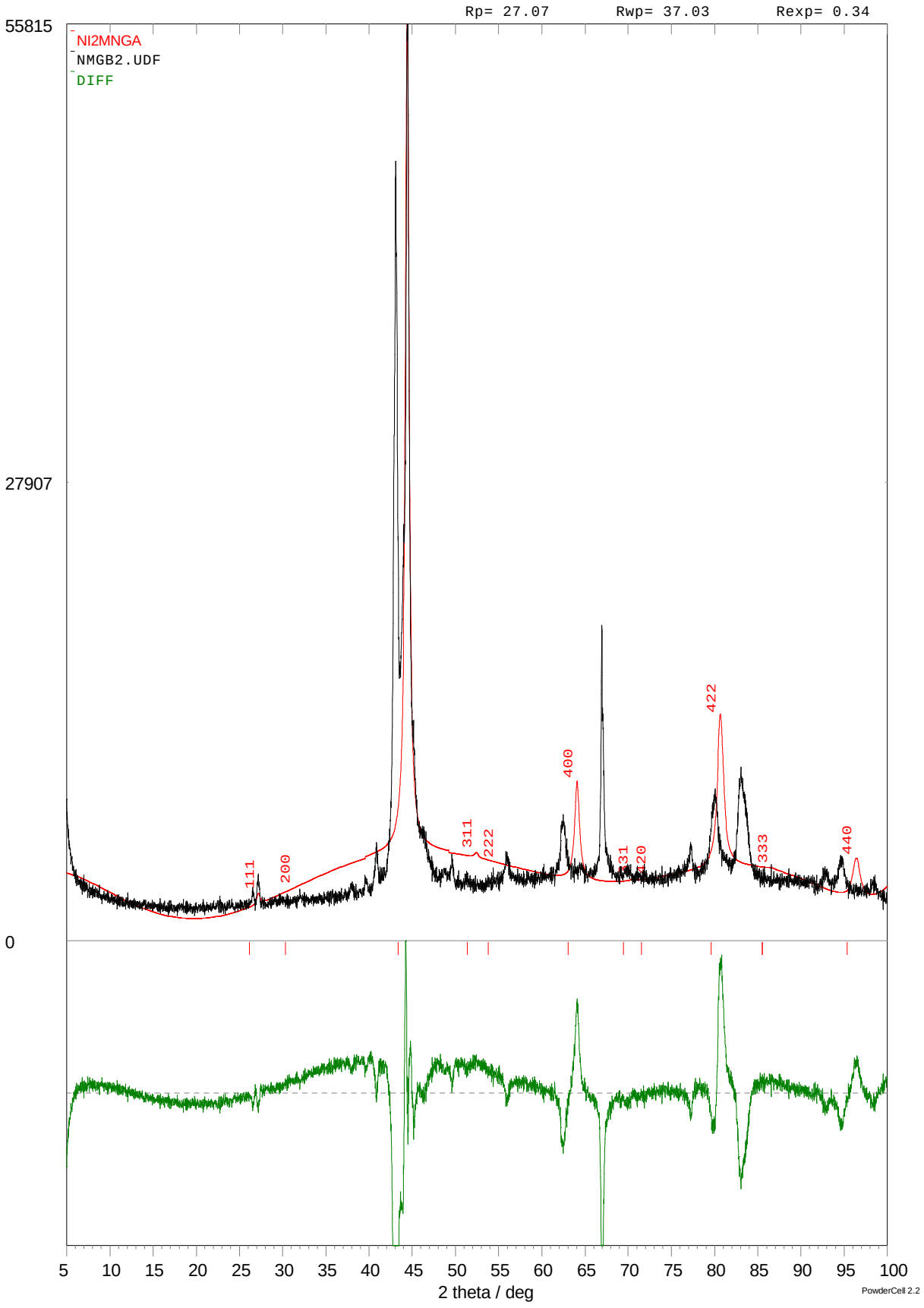

Figure C.2: X-ray diffraction for $Ni_2MnGa_{0,9}Bi_{0,1}$

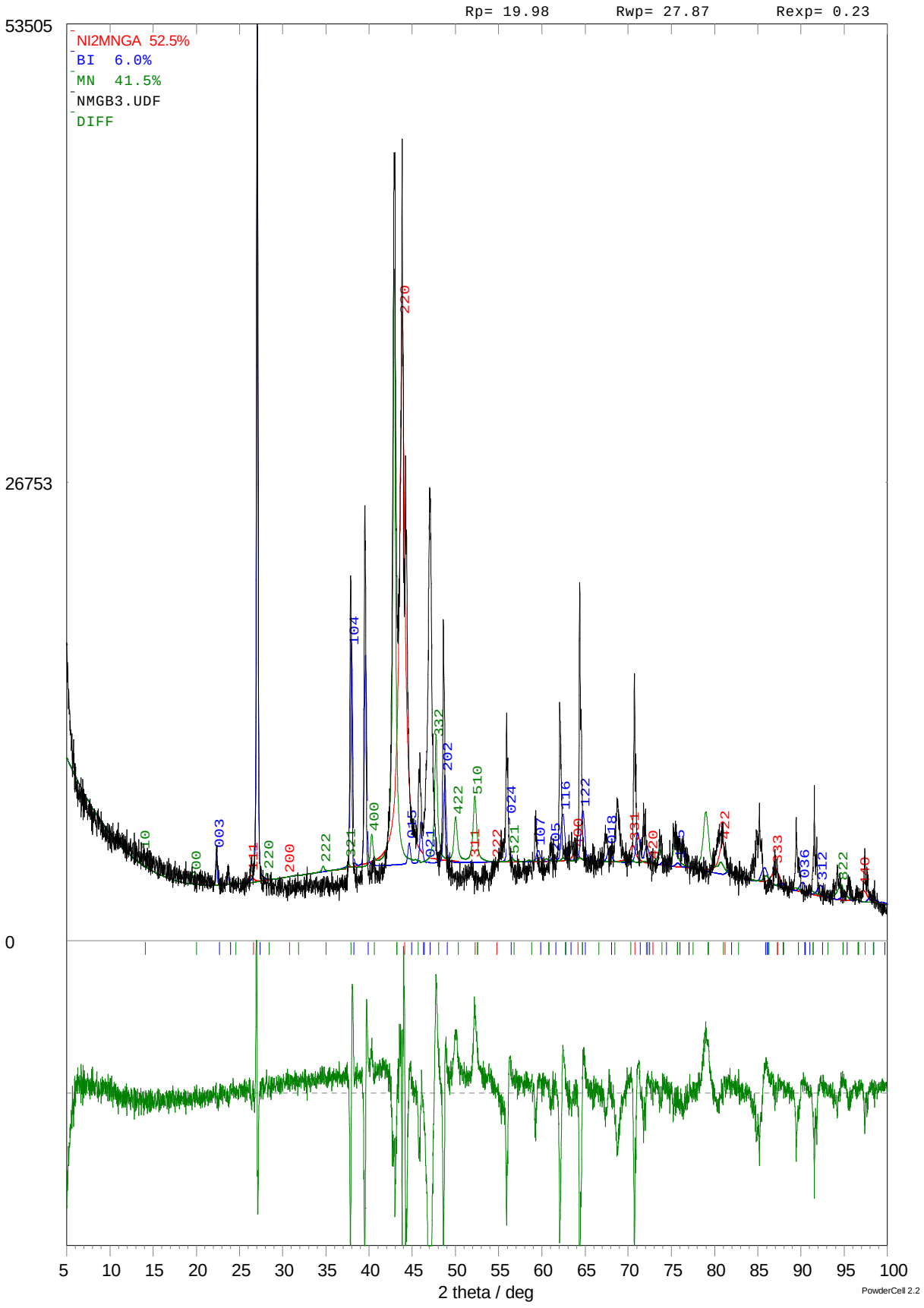

Figure C.3: X-ray diffraction for $Ni_2MnGa_{0,8}Bi_{0,2}$

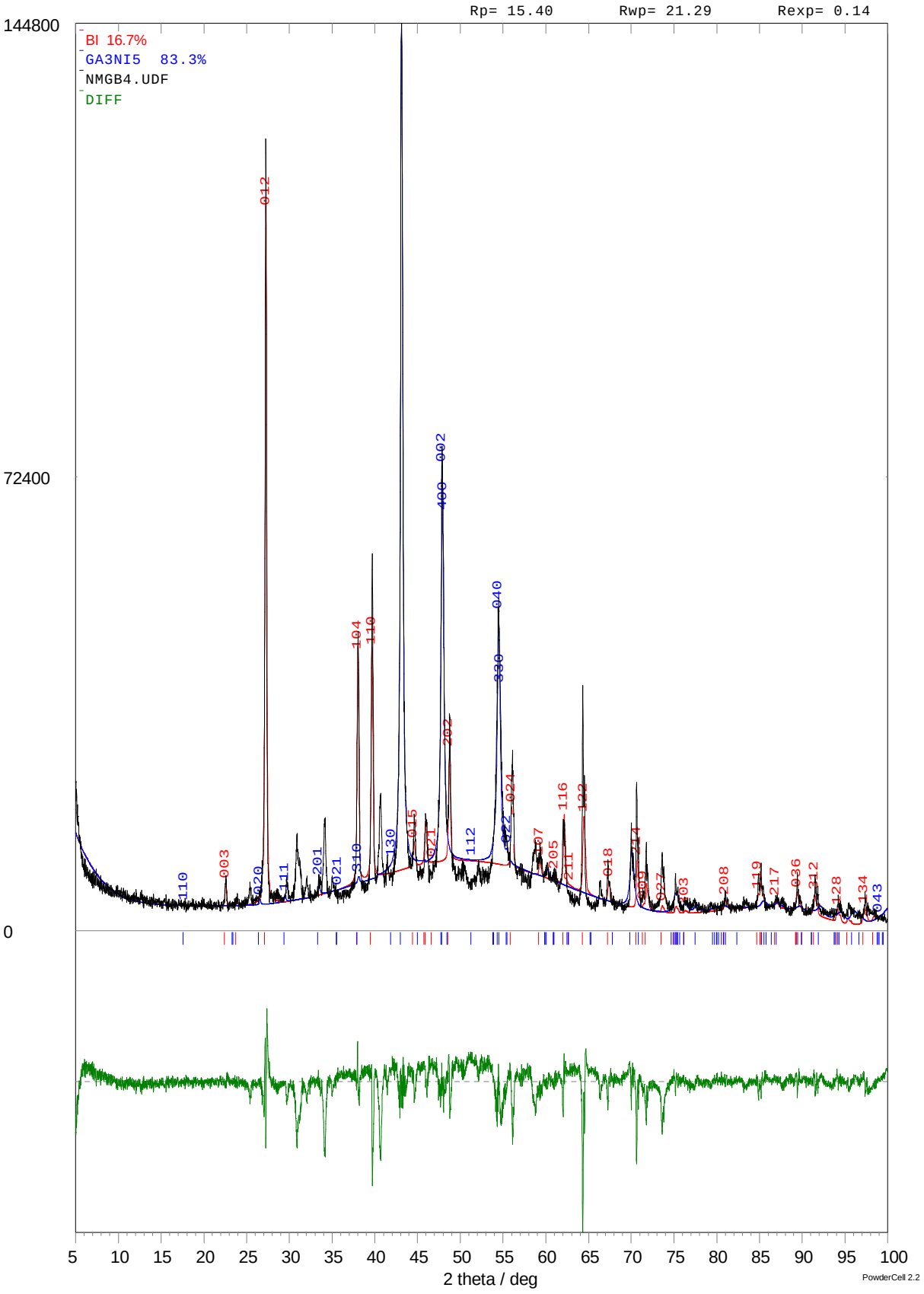

Figure C.4: X-ray diffraction for $Ni_2MnGa_{0,7}Bi_{0,3}$

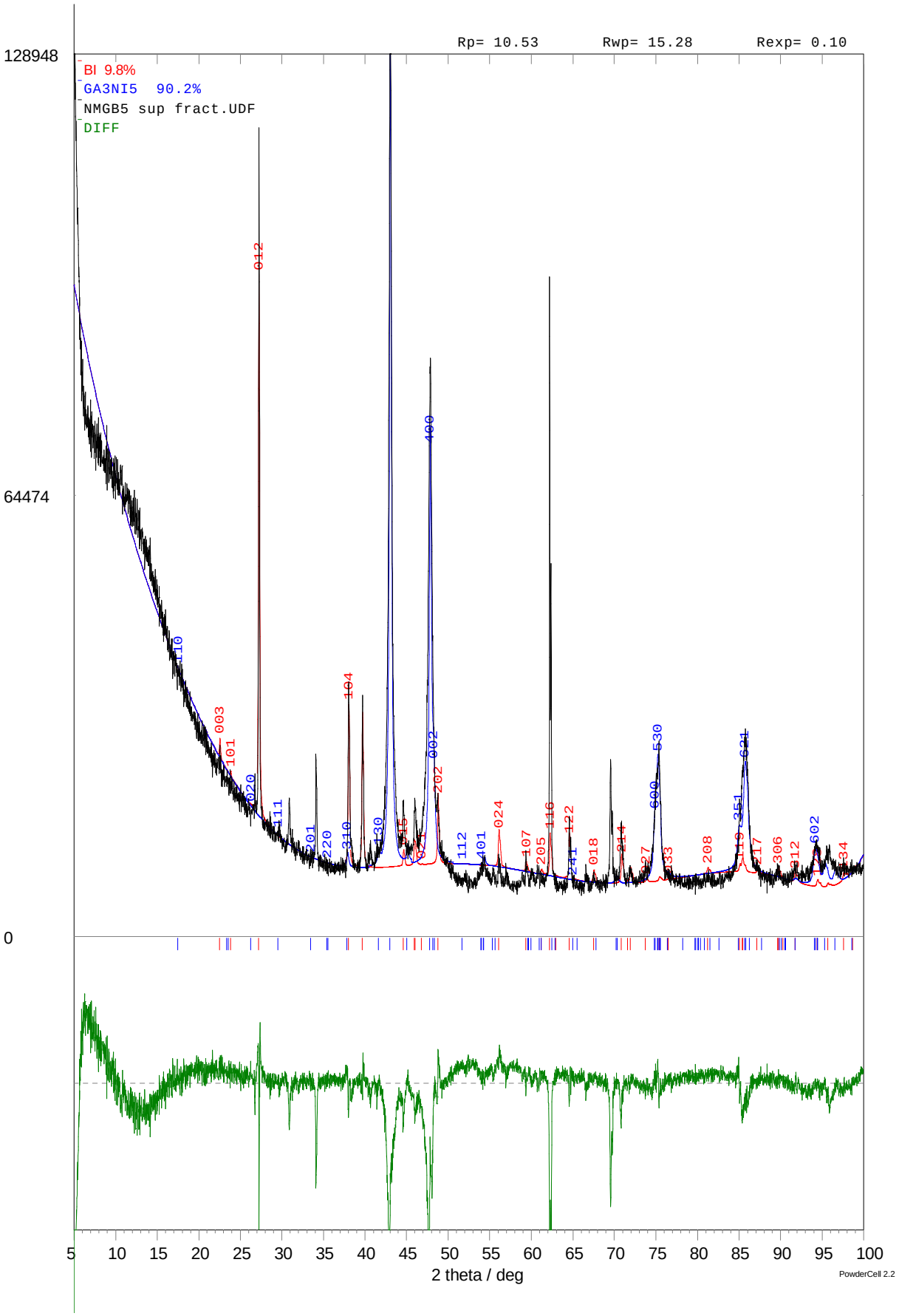

Figure C.5: X-ray diffraction for $Ni_2MnGa_{0,6}Bi_{0,4}$

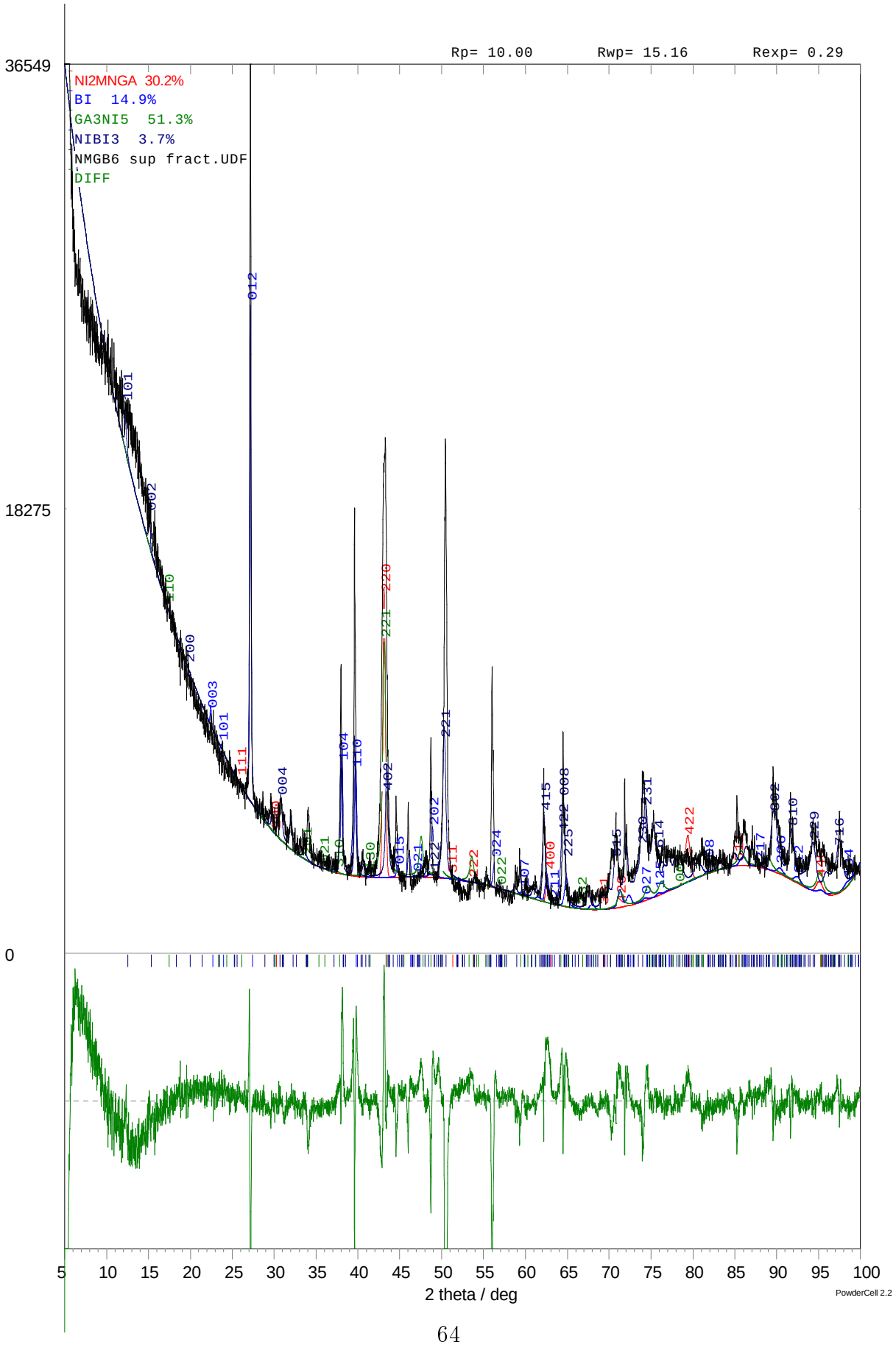

Figure C.6: X-ray diffraction for $Ni_2MnGa_{0,5}Bi_{0,5}$

Apêndice D

Sample SEM photos

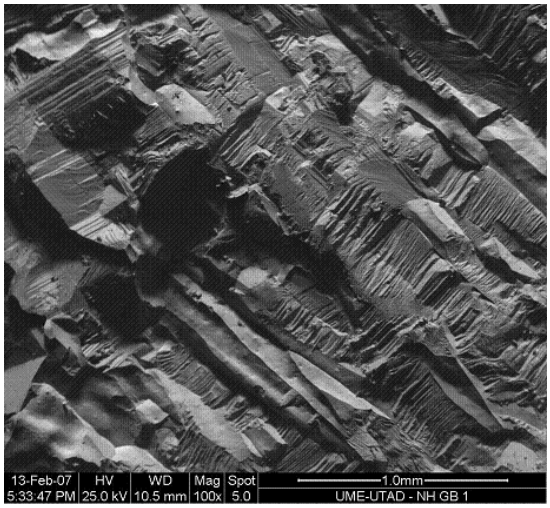

(a) Ni_2MnGa magnification 100x

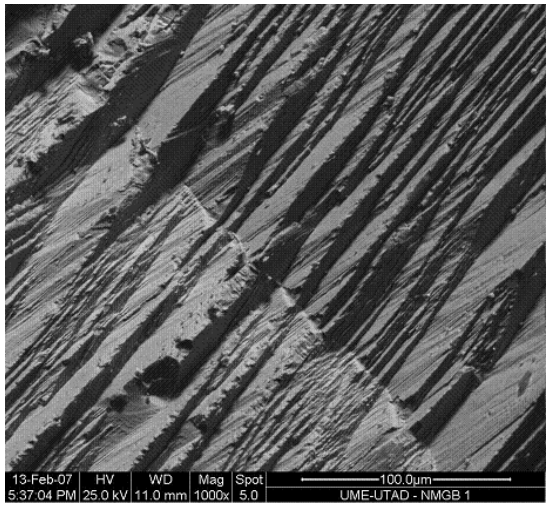

(b) Ni_2MnGa magnification 1000x

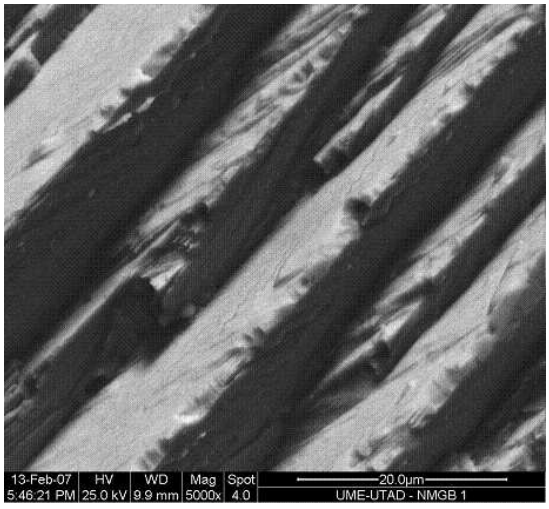

(c) Ni_2MnGa magnification 5000x

Figure D.1: Ni_2MnGa sample SEM photos

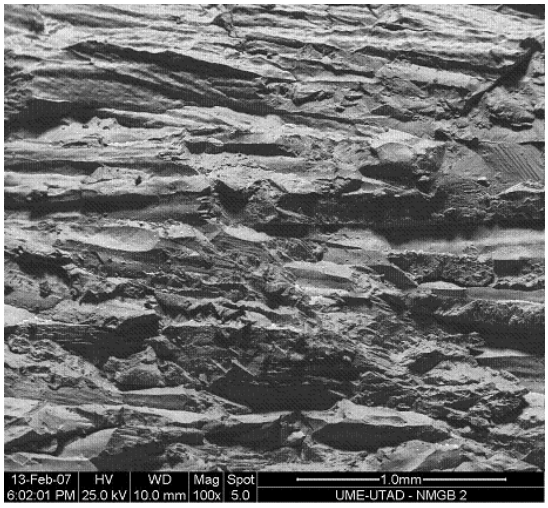

(a) $Ni_2MnGa_{0,9}Bi_{0,1}$ magnification 100x

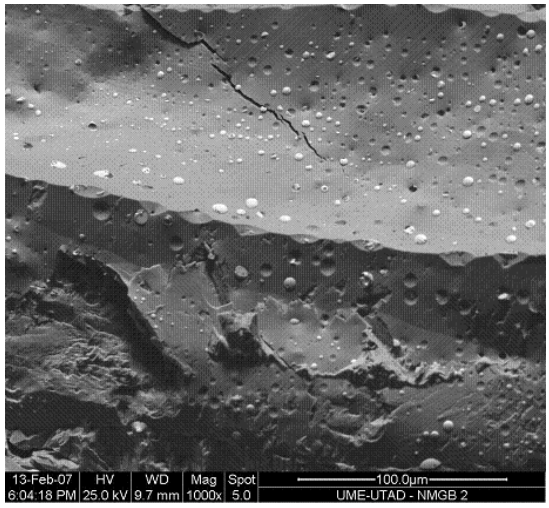

(b) $Ni_2MnGa_{0,9}Bi_{0,1}$ magnification 1000x

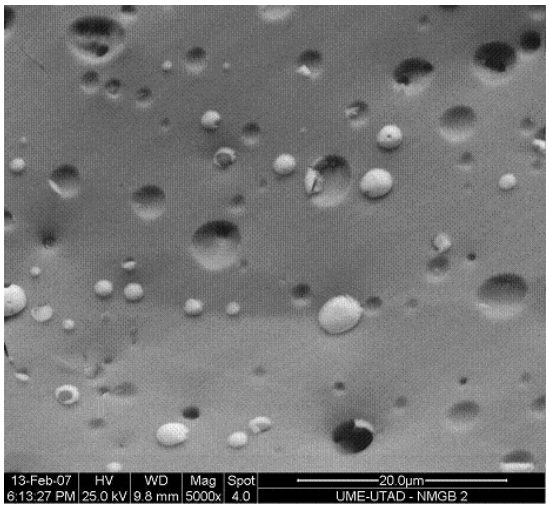

(c) $Ni_2MnGa_{0,9}Bi_{0,1}$ magnification 5000x

Figure D.2: $Ni_2MnGa_{0,9}Bi_{0,1}$ sample SEM photos

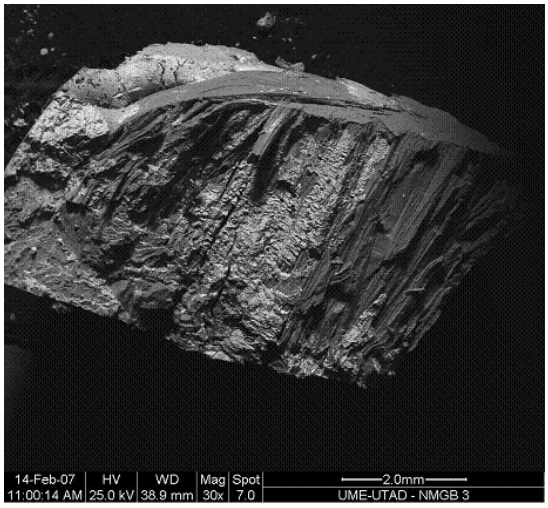

(a) $Ni_2MnGa_{0,8}Bi_{0,2}$ magnification 30x

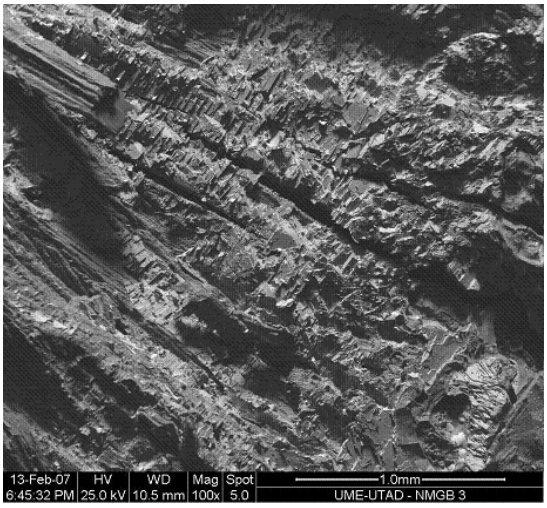

(b) $Ni_2MnGa_{0,8}Bi_{0,2}$ magnification 100x

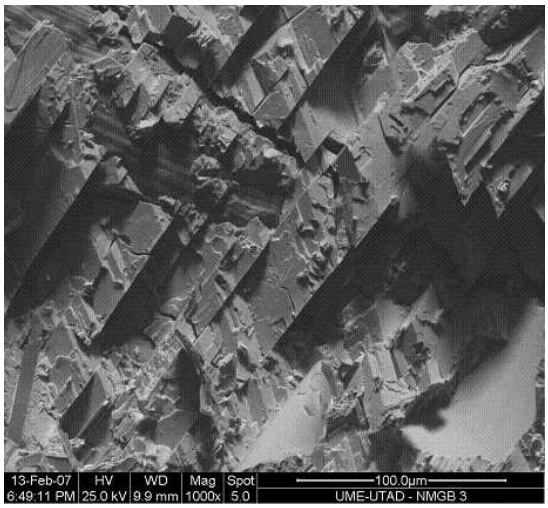

(c) $Ni_2MnGa_{0,8}Bi_{0,2}$ magnification 1000x

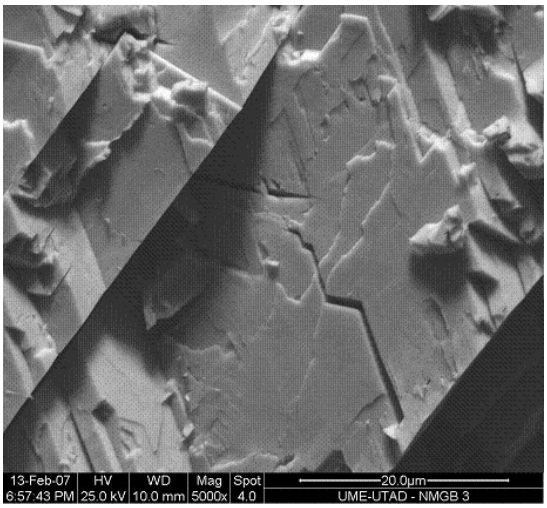

(d) $Ni_2MnGa_{0,8}Bi_{0,2}$ magnification 5000x

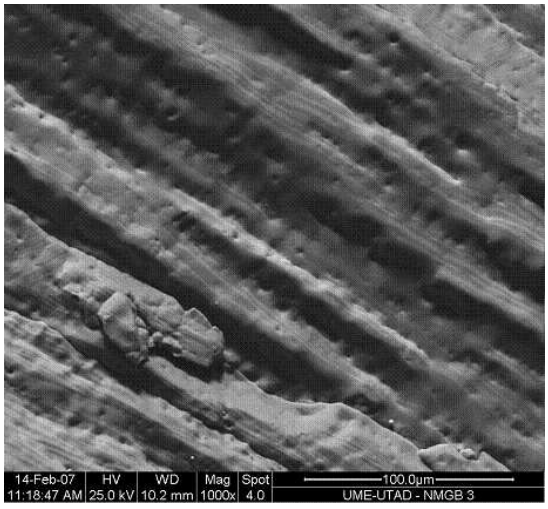

(e) $Ni_2MnGa_{0,8}Bi_{0,2}$ different region magnification 1000x

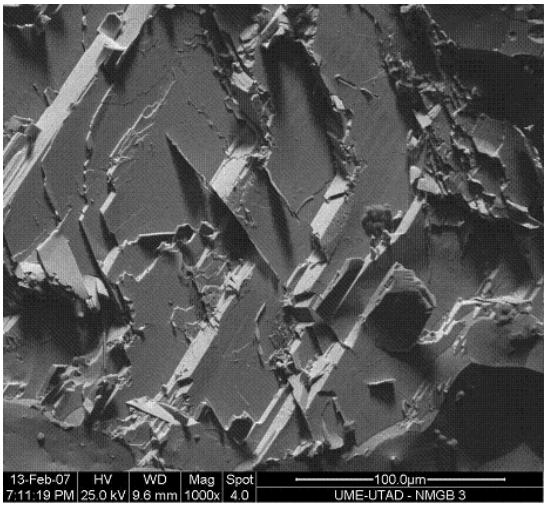

(f) $Ni_2MnGa_{0,8}Bi_{0,2}$ another different region magnification 1000x

Figure D.3: $Ni_2MnGa_{0,8}Bi_{0,2}$ sample SEM photos

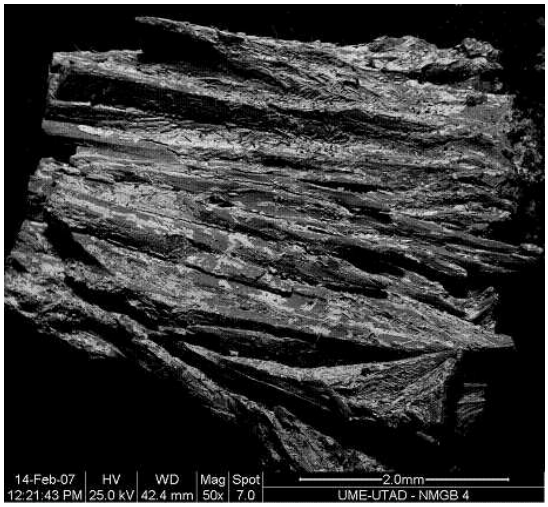

(a) $Ni_2MnGa_{0,7}Bi_{0,3}$ magnification 50x

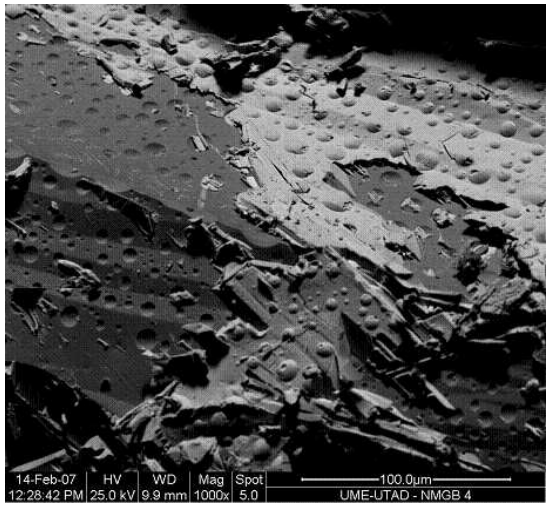

(b) $Ni_2MnGa_{0,7}Bi_{0,3}$ magnification 1000x

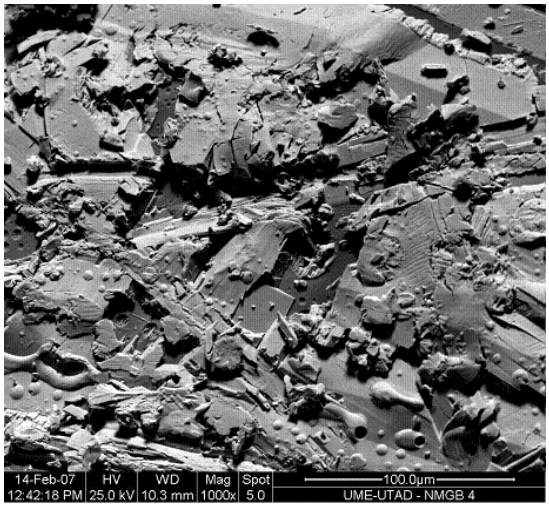

(c) $Ni_2MnGa_{0,7}Bi_{0,3}$ different region magnification 1000x

Figure D.4: $Ni_2MnGa_{0,7}Bi_{0,3}$ sample SEM photos

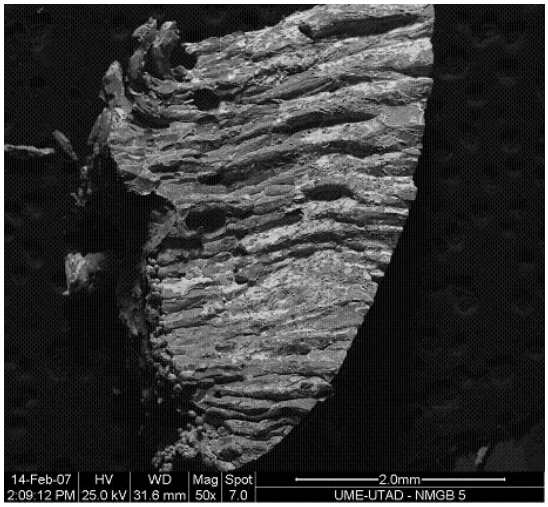

(a) $Ni_2MnGa_{0,6}Bi_{0,4}$ magnification 50x

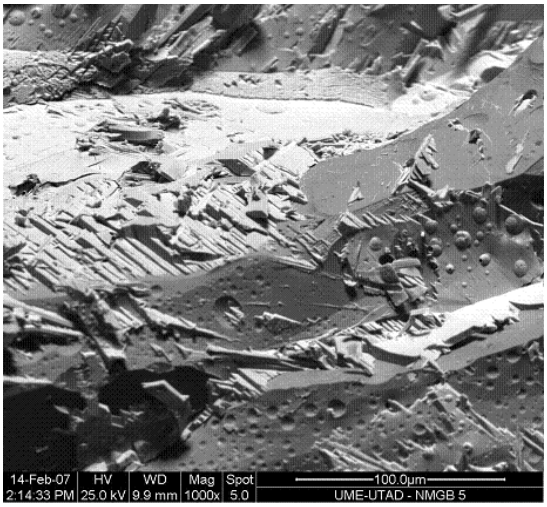

(b) $Ni_2MnGa_{0,6}Bi_{0,4}$ magnification 1000x

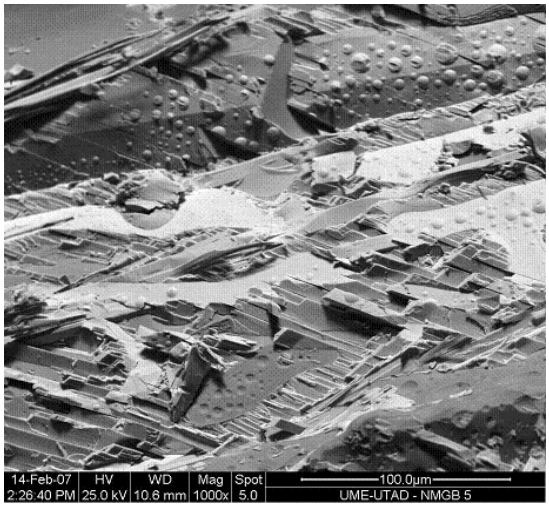

(c) $Ni_2MnGa_{0,6}Bi_{0,4}$ different region magnification 1000x

Figure D.5: $Ni_2MnGa_{0,6}Bi_{0,4}$ sample SEM photos

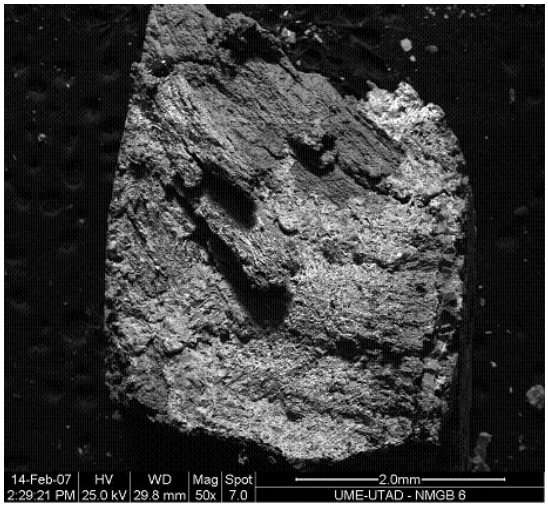

(a) $Ni_2MnGa_{0,5}Bi_{0,5}$ magnification 50x

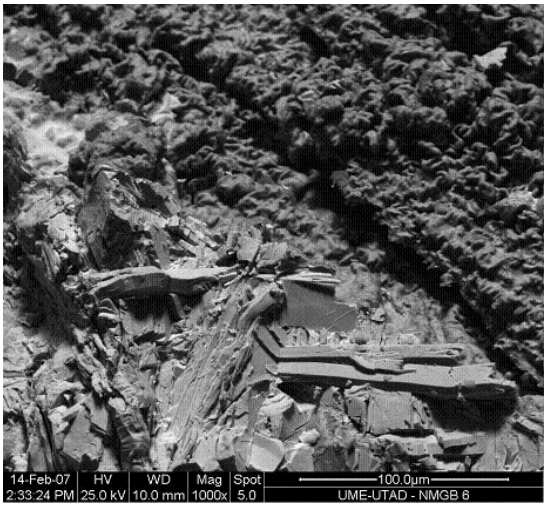

(b) $Ni_2MnGa_{0,5}Bi_{0,5}$ magnification 1000x

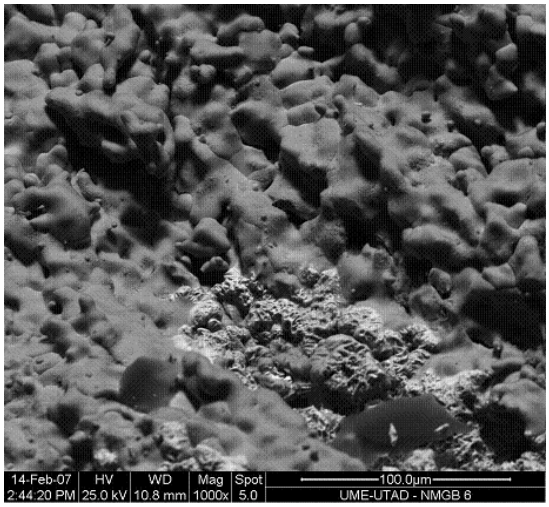

(c) $Ni_2MnGa_{0,5}Bi_{0,5}$ different region magnification 1000x

Figure D.6: $Ni_2MnGa_{0,5}Bi_{0,5}$ sample SEM photos

Bibliography

[1] Nagengast B. *Mech. Eng. Mag.* **May** (2000) 56.

[2] Tsai W.T. *Chemosphere* **61** (2005) 1539.

[3] Fernandes R.P. *Magnetocaloric effect of $Pr(Ni,Co)_5$ hard magnets and $Ni_2Mn(Ga,Bi)$ shape memory alloys* (Universidade de Aveiro, Aveiro, 2007) .

[4] Gschneidner K.A. and Pecharsky V.K. *Annu. Rev. Mater. Sci.* **30** (2000) 387.

[5] Warburg E. *Ann. Phys.* **13** (1881) 141.

[6] Debye P. *Ann. Phys.* **81** (1926) 1154.

[7] Giauque W.F. *J. Am. Chem. Soc* **49** (1927) 1864.

[8] Giauque W.F. and MacDougall D.P. *Phys. Rev.* **43** (1933) 768.

[9] Jr K.A.G., Pecharsky V.K. and Tsokol A.O. *Rep. Prog. Phys.* **68** (2005) 1479.

[10] Guimarães A.P. and Oliveira I. *Magnetism and Magnetic Resonance in Solids* (Wiley-Interscience, New York, 1998) .

[11] Tishin A. and Spichkin Y. *The Magnetocaloric Effect and its Applications* .

[12] Ferreira A.L. *Apontamentos de Física Estatística* (Universidade de Aveiro, Aveiro, 1997) .

[13] Reis M. *Sci. Amer. Br.* **34** (2005) 44.

[14] Pecharsky V.K. and K. A. Gschneidner J. *Phys. Rev. Lett.* **78** (1997) 4494.

[15] Choe W., Pecharsky V.K., Pecharsky A.O., K. A. Gschneidner J., V. G. Young J. and Miller G.J. *Phys. Rev. Lett.* **84** (2000) 4617.

[16] Pecharsky V.K., Holm A.P., K. A. Gschneidner J. and Rink R. *Phys. Rev. Lett.* **91** (2003) 197204.

[17] Morellon L., Arnold Z., Magen C., Ritter C., Prokhnenko O., Skorokhod Y., Algarabel P.A., Ibarra M.R. and Kamarad J. *Phys. Rev. Lett.* **93** (2004) 137201.

[18] Spichkin Y.I., Pecharsky V.K. and K. A. Gschneidner J. *J. Appl. Phys.* **89** (2001) 1738.

[19] Thuy T. *Proc. 8th Asia-Pacific Physics Conf. (Singapore: World Scientific)* **8** (2001) 354.

[20] Morellon L., Magen C., Algarabel P.A., Ibarra M.R. and Ritter C. *Appl. Phys. Lett.* **79** (2001) 1318.

[21] Ivchenko I. *Adv. Cryog. Eng.* **46** (2000) 405.

[22] Thuy N., Chen Y., Yao Y., Wang C., Lin S., Ho J., Nguyen T., Thang P., Klaasse J., Hien N. and Tai L. *J. Magn. Magn. Mater* **262** (2003) 432.

[23] Hu F.X. *J. Phys: Condens. Matter* **12** (2000) 2691.

[24] Fujita A., Fujieda S., Hasegawa Y. and Fukamichi K. *Phys. Rev. B* **67** (2003) 104416.

[25] Fujita A., Fujieda S., Fukamichi K., Mitamura H. and Goto T. *Phys. Rev. B* **65** (2001) 014410.

[26] Fujieda S., Fujita A. and Fukamichi K. *Proceedings of the First IIR International Conf. on Magnetic Refrigeration at Room Temperature, Montreux-Switzerland* (2005) 193.

[27] Wada H. and Tanabe Y. *Appl. Phys. Lett* **79** (2001) 3302.

[28] Gama S., Coelho A.A., de Campos A., Carvalho A.M.G., Gandra F.C., von Ranke P.J. and de Oliveira N.A. *Appl. Phys. Lett* **93** (2004) 237202.

[29] Tegus O., Brück E., Zhang L., Dagula, Buschow K. and de Boer F. *Physica B* **319** (2002) 174.

[30] Hu F.X., gen Shen B. and rong Sun J. *Appl. Phy. Lett.* **76** (2000) 3460.

[31] Zhou X., Li W., Kunkel H.P. and GwynWilliams. *J. Phys: Condens. Matter* **16** (2004) L39.

[32] Morelli D.T., Mance A.M., Mantese J.V. and Micheli A.L. *J. Appl. Phys.* **79** (1996) 373.

[33] Amaral J.S. and Amaral V.S. *J. Magn. Magn. Mater.* **272** (2004) 2104.

[34] Chen H., Lin C. and Dai D. *J. Magn. Magn. Mater.* **257** (2003) 254.

[35] Reis M.S., Amaral V.S., Araújo J.P., Tavares P.B., Gomes A.M. and Oliveira I.S. *Phys. Rev. B* **71** (2005) 144413.

[36] Chen P., Du Y.W. and Ni G. *Europhys. Lett.* **52** (2000) 589.

[37] Wang D., Liu H., Tang S., Yang S., Huang S. and Du Y. *Phys. Lett. A* **297** (2002) 247.

[38] de Oliveira N.A., von Ranke P.J. and Troper A. *Phys. Rev. B* **69** (2004) 064421.

[39] von Ranke P.J., Nóbrega E.P., de Oliveira I.G., Gomes A.M. and Sarthour R.S. *Phys. Rev. B* **63** (2001) 184406.

[40] Dan'kov S., Ivtchenko V., Tishin A., K.A. Gschneidner J. and Pecharsky V. *Adv. Cryog. Eng.* **46** (2000) 397.

[41] Canepa F., Napoletano M. and Cirafici S. *Intermetallics* **10** (2002) 731.

[42] Niua X., Jr. K.G., Pecharskya A. and Pecharsky V. *J. Mag. Mag. Mater.* **234** (2001) 193.

[43] Ilyn M.I., Tishin A.M., K A Gschneidner J., Pecharsky V.K. and Pecharsky A.O. *Cryocoolers 11 ed R G Ross Jr (New York: Kluwer/Plenum)* (2001) 457.

[44] Hu F.X., rong Sun J., heng Wu G. and gen Shen B. *Jour. App. Phy.* **90** (2001) 5216.

[45] Pasquale M., Sasso C.P. and Lewis L. *Jour. App. Phy.* **95** (2004) 6918.

[46] Marcos J., Planes A., Mañosa L., Casanova F., Batlle X., Labarta A. and Martínez B. *Phys. Rev. B* **66** (2002) 224413.

[47] Aliev A., Batdalov A., Bosko S., Buchelnikov V., Dikshtein I., Khovailo V., Koledov V., Levitin R., Shavrov V. and Takagi T. *Jour. Magsm. Mag. Mat.* **272-276** (2004) 2040.

[48] Zhou X., Li W., Kunkel H. and Williams G. *Journ. Phys. Cond. Mat.* **16** (2004) 39.

[49] Khovailo V., Takagi T., Tani J., Levitin R., Cherechukin A., Matsumoto M. and Note R. *Phys. Rev. B* **65** (2002) 92410.

[50] Albertini F., Canepa F., Cirafici S., Franceschi E., Napoletano M., Paoluzi A., Pareti L. and Solzi M. *Jour. Magn. Magn. Mat.* **272-276** (2003) 2111.

[51] Khovailo V., Novosad V., Takagi T., Filippov D., Levitin R. and Vasil'ev A. *Phys. Rev. B* **70** (2004) 174413.

[52] Vasil'ev A., Bozhko A., Khovailo V., Dikshtein I., Shavron V., Buchelnikov V., Matsumoto M., Suzuki S., Takagi T. and Tani J. *Phys. Rev. B* **59** (1999) 1113.

[53] Stadler S., Khan M., Mitchell J., Ali N., Gomes A.M., Dubenko I., Takeuchi A.Y. and Guimarães A.P. *Ap. Phy. Lett* **88** (2006) 192511.

[54] Gomes A.M., Khan M., Stadler S., Ali N., Dubenko I., Takeuchi A.Y. and Guimarães A.P. *Jour. Ap. Phy* **99** (2006) 08Q106.

[55] Söderberg O., Koho T., Sammi T., Liu X., , Sozinov A., Lanska N. and Lindroos V. *Mat. Sci. Eng. A* **378** (2003) 389.

[56] Brück E. *Jour. Phy. D: Ap. Phy.* **38** (2005) R381.

[57] Brück E., Tegus O., Thanh D. and Buschow K. *Jour. Magn. Magn. Mat.* **310** (2007) 2793.

[58] xia Hu F., gen Shen B., rong Sun J. and heng Wu G. *Phys. Rev. B* **64** (2001) 132412.